Doctoral Thesis for the Degree of Doctor of Philosophy, Faculty of Medicine

Identification and imaging of lipids in tissues using TOF-SIMS

Ylva Magnusson

Wallenberg Laboratory
Department of Molecular and Clinical Medicine, Institution of Medicine,
Sahlgrenska Academy, at Göteborg University
Göteborg, Sweden

2008

Doctoral Thesis for the Degree of Doctor of Philosophy, Faculty of Medicine
Identification and imaging of lipids in tissues using TOF-SIMS

Ylva Magnusson

ISBN 978-91-628-7470-4

Doktorsavhandling
Department of Molecular and Clinical Medicine,
Institution of Medicine,
Sahlgrenska Academy, at Göteborg University
Göteborg, Sweden 2008

Printed by Chalmers Reproservice
Göteborg, 2008

Identification and imaging of lipids in tissues using TOF-SIMS

Ylva Magnusson

**Department of Molecular and Clinical Medicine, Institution of Medicine,
Sahlgrenska Academy, at Göteborg University
Göteborg, Sweden. Thesis defended 11 april, 2008**

Abstract

Introduction: Normal lipid metabolism in the adipose tissue, skeletal muscle and aortic wall is important for the physiological function of these tissues. Dyslipidemia that is often associated with intake of high energy diet and sedentary lifestyles can lead to the development of insulin resistance and cardiovascular diseases. Existing methods for imaging the heterogeneous distribution of lipids in the skeletal muscle and adipose tissue is limited. Our aim is to, without probing and chemical fixation, identify and image the spatial distribution of lipids in the skeletal muscle, adipose tissue and aorta, and to reveal an altered lipid pattern in the skeletal muscle associated with obesity and in the aorta associated with high glucose intake. To achieve this, we used time-of-flight secondary-ion mass spectrometry (TOF-SIMS) equipped with a bismuth (Bi)-cluster gun which is a new technique for molecular imaging of biological samples. Principal component analysis (PCA) was used for studying changes between experimental and control groups.
Methods: Human adipose and skeletal muscle tissue were obtained from obese youths and aortas were taken from Wistar Rats with or without glucose drinking. The samples were prepared by high pressure freezing, freeze-fracturing. Gastrocnemius skeletal muscle was taken from obese ob/ob mice and lean wild-type mice. The tissue was cryofixed and cryosectionized. All samples were dehydrated by a freeze drying process in ultra high vaacum. The tissue was analyzed by TOF-SIMS. Semi-quantitative measurements in the rat aorta and in the mice skeletal muscle were based on principal component analysis.
Results: In the negative spectra, we identified fatty acids and triacylglycerol. In the positive spectra, we identified the phosphocholine, cholesterol and diacylglycerol. Heterogeneous distribution of these molecules was observed in the skeletal muscle and adipose tissue. By using PCA, we identified a reduced signal of cholesterol in rats with high glucose intake compared to control rats. The obese ob/ob mice showed an increased level of fatty acids and diacylglycerol. The ratio between fatty acid peaks showed changed fatty acid composition in the rat aorta associated with high glucose intake and in the mice skeletal muscle associated with obesity.
Conclusions: With the help of imaging TOF-SIMS, it is possible to depict the heterogeneous localization of fatty acids, phosphocholine, cholesterol, diacylglycerol and triacylglycerol in the adipose tissue, skeletal muscle and aortic wall. Moreover, imaging TOF-SIMS together with PCA analysis of TOF-SIMS spectra is a promising tool for studying lipid alterations in tissues.

LIST OF PAPERS

This thesis is based on the following papers, which will be referred to in the text by their roman numerals:

I: Per Malmberg, Håkan Nygren, Katrin Richter, Yun Chen, Frida Dangardt, Peter Friberg and Ylva Magnusson. Imaging of Lipids in Human Adipose Tissue by Cluster Ion TOF-SIMS. Microscopic research and technique, 2007 Volume 70, Issue 9 828-835

II: Ylva Magnusson, Peter Friberg, Peter Sjövall, Frida Dangardt, Per Malmberg and Yun Chen. Lipid imaging of human skeletal muscle using TOF-SIMS with Bismuth cluster ion as a primary ion source. Clinical Pysiology and functional imaging (In press)

III: Ylva Magnusson, Peter Friberg, Per Malmberg, Håkan Nygren and Yun Chen. Application of multivariate analysis of TOF-SIMS spectra for styding the effect of high glucose intake on aortic lipid profile
Submitted

IV: Ylva Magnusson, Peter Friberg, Peter Sjövall, Jakob Malm and Yun Chen. TOF-SIMS analysis of lipid accumulation in the skeletal muscle of ob/ob mice
Submitted

LIST OF CONTENTS

ABBREVIATIONS

ADRP	Adipose differentiation- related protein
DAG	Diacylglycerols
DGLA	Dihomo-gamma linolenic acids
EM PACT	High-pressure freezing machine
ER	Endoplasmic reticulum
FAS	Fatty acid synthetase
FFA	Free fatty acids
HPF	High-pressure frozen
IMCL	Intramyocellular lipids
LMIG	Liquid metal ion gun
LN2	Liquid nitrogen
MALDI-MS	Matrix-assisted laser desorption/ionization mass spectrometry
MRS	Magnetic Resonance Spectroscopy
MUFA	Monounsaturated fatty acids
m/z	Mass to charge ratio
PC	phosphatidylcholine
PCh	Phosphocholine
PC1	Principal Component 1
PCA	Principal Component Analysis
PUFA	Polyunsaturated fatty acids
SEM	Scanning electron microscopy
SIMS	Secondary Ion Mass Spectrometry
TAG	Triacylglycerol
TLC	Thin Layer Chromatography
TOF-SIMS	Time-of-flight secondary ion mass spectrometry

“Ad extremum”

INTRODUCTION

Obesity induced by sedentary lifestyle and energy-rich diet is an increasing problem around the world. Millions of people are suffering from overweight, a problem which is hazardous to their health and leading to premature death. Obese animals and humans accumulate lipids not only in the adipose tissue, but also in other tissues such as the liver, skeletal muscle and the aortic wall. This so-called non-ectopic lipid accumulation is a strong contributor to the development of insulin resistance, type-2 diabetes and cardiovascular disease [1-4]. On the basis thereof, it is necessary to further investigate the lipid distribution pattern in those tissues. Time-of-flight secondary ion mass spectrometry (TOF-SIMS) with the use of Bismuth clustering ions is an imaging mass spectrometry method with high lateral resolution, which permits identification and localization of lipids without probing and chemical fixation. This method provides information about the chemistry of tissue samples, and represents a new approach for identifying and imaging lipids in biological tissues.

Dyslipidemia and Insulin resistance

Insulin, a protein hormone produced by pancreatic β-cells is needed for the control of both carbohydrate and lipid metabolism [5]. Consequently, failure in insulin signalling has widespread and devastating effects on many organs. When the amount of insulin is insufficient to produce a physiologically adequate insulin response from fat, muscle and liver cells, insulin resistance develops [6,7]. As a result, the possibility to store lipids within the adipose tissue fails. The free fatty acid (FFA) uptake by the adipose tissue is decreased and the stored triacylglycerol (TAG) is hydrolyzed. This causes an augmented FFA release by the adipocytes, resulting in elevated plasma FFA [8,9]. When excess FFA is transported to the skeletal muscle, this will lead to lipid overloading in muscle cells which will prevent glucose uptake and utilization [10,11]. More specifically, accumulation of intermediates of lipid metabolism, such as diacylglycerol (DAG) and Acyl-CoA has been shown to interfere with insulin signalling [12]. In the liver, high FFA level decreases its ability to store carbohydrates, which consequently leads to elevated blood glucose. High plasma insulin levels of and glucose due to insulin resistance often lead to metabolic syndrome with an increased risk of both atherosclerosis and type-2 diabetes[13-15] .

Lipids

The primary function of lipids in biological systems is to store energy, predominately in the form of TAG. Lipids are also the important integral components in the cell membrane, and they can act as secondary messengers in signal transduction or produce prostaglandins. Further, other purposes of lipids are to function as vitamins and hormones. Choline is an amine originated in the lipids. Choline is vital for the build up signalling functions of cell membranes, and in the formation of phosphocholine as reviewed by Vance et Vance [16]. Abnormal lipid metabolism is strong contributors to insulin resistance, type-2 diabetes and cardiovascular diseases. For example, in obesity many studies show that both saturated fatty acid (SFA), and monounsaturated fatty acids (MUFA) are upregulated, and that polyunsaturated fatty acid (PUFA) are decreased [17].

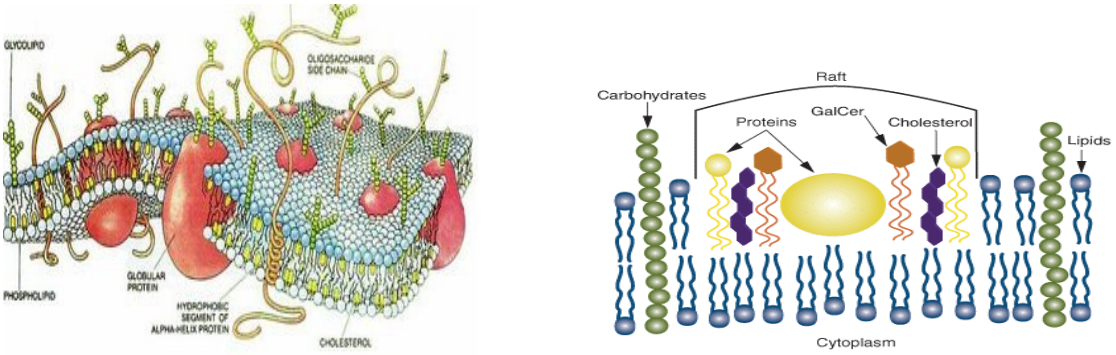

Figure 1 a) Cellular membrane b) Lipid raft component

Phospholipids

The glycerol-based phospholipids (e.g. glycerophospholipids) constitute one of the most abundant structural components of biological membranes. Together with cholesterol and glycolipids (e.g.sphingolipids) they create an essential milieu of cellular membranes (Fig.1a) [18,19]. The saturation degree of fatty acid residues of phospholipids determines the membrane fluidity which in turn directly affects most cellular processes Several double bonds provide the fatty acid chain with an unregular form which is affecting the melting point [16,20]. This has a major impact in different disease states including diabetes, obesity, and heart diseases [21]. SFAs, such as stearic acid (C18:0), are likely to contribute to the rigidity of membranes, since they can be packed tightly in the phospholipid membrane [22]. Both sphingomyelins and phosphatidylcholine contain phosphocholine as the polar head group, but

their hydrophobic backbone is different. Sphingomyelin synthesis involves the transfer of phosphocholine from phosphatidylcholine onto ceramide, producing DAG as a by-product [23].

DAG

DAG is a glyceride with two fatty acids esterfied with a glycerol molecule produced from glycerol-3-phosphate pathway [24,25] or synthesised from acylation of monoacylglycerol [26]. DAG can be further converted to phosphatidylcholine and phosphatidyletanolamine or TAG [16]. DAG is not a major component of biological membranes, but plays a significant role in both intermediate metabolism and in signal transduction as a second messenger and has been shown to accumulate in the insulin-resistant muscle of high-fat fed rats [27,28]. Increased levels of DAG may be due to chronic hyperinsulinemia or by hydrolysis of phosphatidylcholine.

Cholesterol

Cholesterol is another lipid that plays a major role in the membrane structure. However, excessive cholesterol is involved in the formation of atherosclerotic lesions [16]. Cholesterol is transported in the plasma predominantly as cholesteryl esters associated with lipoproteins [29]. Acetyl-CoA derived from fatty acids or pyruvate in mitochondria β-oxidation is utilized in cholesterol biosynthesis. A dynamic clustering of sphingolipids and cholesterol forms rafts in the lipid bilayer (see figure 1b) [30]. Lipid raft appears to be a mechanism to group various processes on the cell surface by bringing together various receptor mediated signal transduction processes [31].

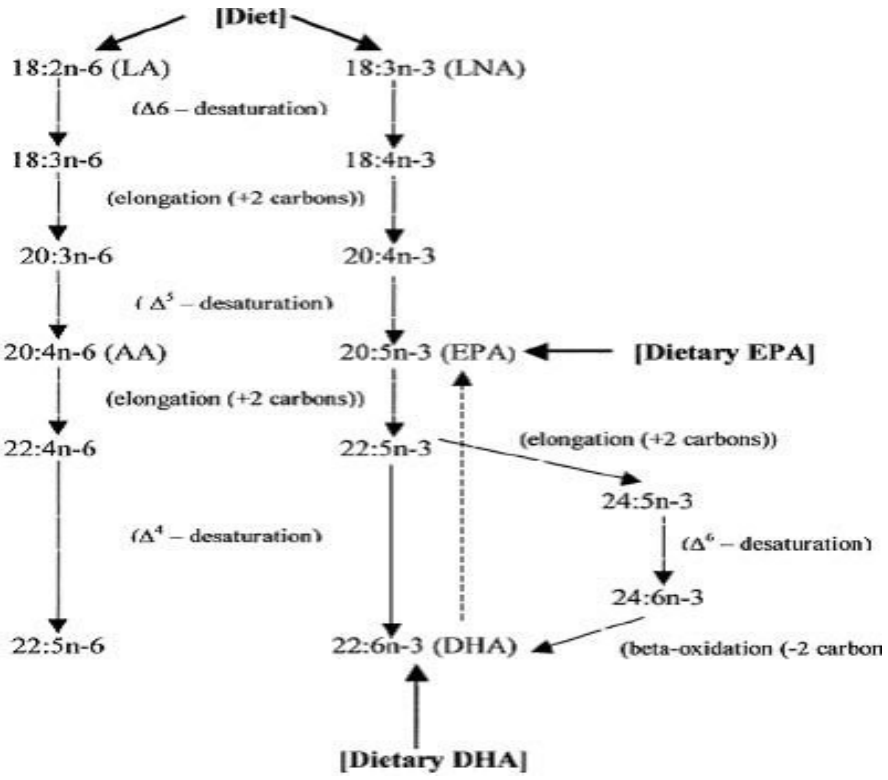

Figure 2 Illustration over chain elongation and desaturation of fatty acids

Chain elongation and desaturation of fatty acids

Fatty acids are a major source of energy in β-oxidation in animals. Fatty acids are also the intermediate in the synthesis of phospholipids and eicosanoid, DAG and TAG. TAG is built up by a glycerol backbone and three esterfied fatty acids. The fatty acid composition of TAG reflects the diet. In animals, the composition tends to be simple, with C16 (mainly 16:0) and C18 (mainly C18:1) fatty acids predominating. If one of the fatty acids in TAG is replaced by a phosphate group, a phospholipid is obtained. There are three major groups of fatty acids; saturated fatty acid (SFA), mono unsaturated fatty acid (MUFA) and polyunsaturated fatty acid (PUFA). New synthesis of fatty acids starts with palmitic acid (C16:0) and some stearic acid (C18:0). C16 and C18 fatty acids are the major components of many membrane lipids. However, long-chain fatty acids are also seen. In myelin for example, over 60% of fatty acids are 18 carbons or longer, and in sphingolipids 24 carbon acyl chains are well-known. Chain lengths of 28-36 carbon have been reported in the phospholipids of the retina photoreceptors [32]. Elongation of fatty acids from palmitic acid (C16:0) requires an elongation enzyme [33]. In eukaryotes, the production of very-long-chain SFA, PUFA (C20 – C26) takes place

independently of fatty acid synthetase (FAS) by membrane-bound elongases on the cytosolic face of the endoplasmic reticulum (ER) membrane [34]. Fatty acid desaturase introduces double bound specific locations in the acyl-chain. By successive actions of elongase and desaturase enzymes the fatty acid chains decide the physiological properties of the membrane function. There are three different desaturase occurring in mammals: delta 9 desaturase, delta 6 desaturase and delta 5 desaturase. The delta 9 desaturase, is also known as stearoyl-CoA desaturase -1 (SCD-1) and is used to synthesize palmitoleic (C16:1) and oleic acid (C18:1) by insertion of a cis-double bond in the delta 9 position of the fatty acid chain. The delta 6 and delta 5 desaturase are required for the synthesis of PUFA such as arachidonic acid, eicosapentanoic acid (EPA) and docosahexaenoic acid (DHA), where alpha-linolenic acid (ALA; 18:3n–3) are the precursor for EPA and DHA. While, arachidonic acid is synthesized from linoleic acid (LA; 18:2 n-6) and is the precursor for prostaglandins [35-37]. All the essential fatty acids, such as linolenic and -linolenic acid, must come from the diet, since mammals are incapable of producing these fatty acids by themselves.

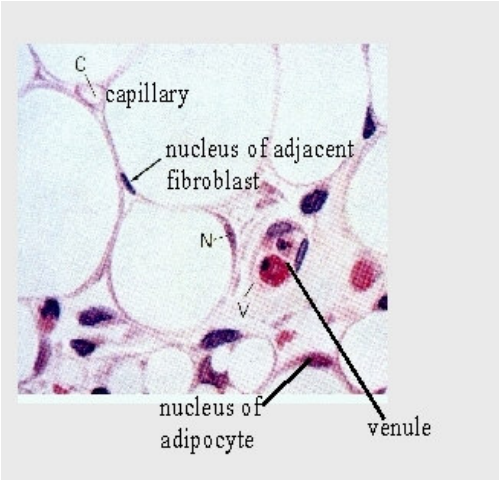

Figure 3 Illustration of the adipose tissue

The Adipose tissue

The characteristics

Adipose tissue is a loose connective tissue composed of adipocytes in an abundant capillary bed; this was known as early as 1850 in work by Fleming [38]. In the middle of 1900 Mirski and co-workers found the adipose tissue to be an active organ with a specific carbohydrate metabolism [39], and at the same time Reynolds and Marble found the lipolytic activity of the adipose tissue in rat and man [40]. Histochemical techniques and chemical analysis showed that insulin increased glycogen synthesis in this tissue [41]. Del Vecchio et al showed the distribution and concentrations of cholesterol in skeletal muscle and adipose tissue [42]. Adipose tissue involvement in insulin resistance and obesity was recognized by Rabinowitz in 1960 [43]. However, since the introduction of the gas-liquid chromatography technique the same decade, more detailed information has been obtained. Hirsch, Hegsted and co-workers showed the fatty acid composition of the adipose tissue in different region of the body [44]. Siiteri et al identified the adipose tissue as a major site for metabolism of sex steroids (i.e. estrogens and cortisone/cortisol) [45]. In the middle of the 1990's, the hormone leptin was identified to be produced by the adipocytes. Hence, the adipose tissue was considered as an endocrine organ [46]. Today, the adipose tissue is established as a complex and highly active metabolic and endocrine organ, which is releasing a number of hormones such as tumor necrosis factor-alpha (TNF-α), Interleukin-6 (IL-6) and adiponectin [47-49] .

The lipid metabolism

The lipid droplet is endured by a core of lipids, which mostly consists of TAG (90-99%) and to a lesser amount of DAG, FFA, phospholipids and monoacylglycerol. The oleic acid (47%) and palmitic acid (19%) are the dominate fatty acids [50]. However, variation in the dietery fatty acid composition can change the fatty acid profile in the adipose tissue. The concentration of DAG in the adipocyte is 1% of the total lipid amount. In addition to their TAG storage, the adipocytes are a deposit for unesterified cholesterol [51,52]. There is approximately 1-5 mg cholesterol per 1g of TAG [53]. The unesterified cholesterol is mainly situated in the cholesterol-rich ER-like surface structures in the cell membrane [54-56]. This might function as a membrane pool to maintaining a stiff cellular membrane because the cell is expanding rapidly [51]. When the adipocyte is enlarging due to increased TAG loading the cholesterol follows, a smaller portion are found as cholesteryl esters in the lipid droplets, surrounded by an amphipathic monolayer of phospholipids [57]. The adipocytes are able to synthesize cholesterol from acetate and mevalonate, which has been shown in rats [58]. There are also specific proteins in the adipose tissue; perilipins and adipose differentiation- related protein (ADRP) to mention some of them [59], and a nucleus pressed in the periphery. The lipid droplets form rapidly in response to elevated fatty acid levels [60]. It has been shown that lipid droplets form from discrete regions of the ER [61] and expand independent of the TAG accumulation, after assembled due to a fusion process which requires intact microtubules [62]. Intake of carbohydrate diet leads to glycogen synthesis by the liver. However, only a few grams of glucogen can be stored before lipogenesis starts. TAG made by the lipogenesis is transported from the liver by apolipoprotein (VLDL or chylomicrons) in the blood plasma [63]. TAGs are hydrolyzed by lipases (LPL) to fatty acids [64], and fatty acid are transported into the adipocyte. Once in the cell, fatty acids esterify onto glycerides at rates dependent upon chain length and degree of unsaturation, and stored as TAG. Glycerol is the building block for TAGs in tissues other than adipose tissue but oxidation of glucose is necessarily performed in the adipocytes as they lack the enzyme glycerol kinase and use dihydroxyacetone phosphate as the precursor for TAG synthesis [65]. The main function of the adipose tissue is to provide a long-term energy reserve of, fatty acids that can be release for oxidation in other organs during food deprivation. Fatty acids are released from TAG by a hormone-sensitive lipase which is activated by phosphorylation dependent on protein kinase A (PKA) [66].

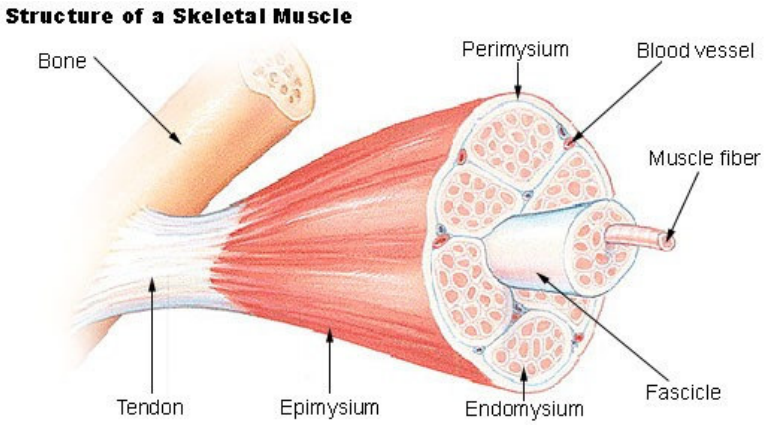

Figure 4 Illustration of the skeletal muscle

The skeletal muscle

The structure

The skeletal muscle consists of two main muscle fibre types, the red oxidative slow-twisted type I and the white fast-twisted fibres type II (a, and b) according to their amount of myoglobin and their mechanism to produce ATP [55,67]. In general, the type I muscle fibre has a greater oxidative metabolism, a greater lipid content and are more insulin-sensitive than the type II muscle fibre [13,68].

Lipid metabolism

The skeletal muscle uses FFA and glucose as substrate. Fat utilization by muscle was first shown in 1952 by Wertheimer et al [69]. The skeletal muscle is a major site of insulin action and relations between the fatty acid composition of phospholipids in skeletal muscle and insulin sensitivity have been reported [70]. In 1963, Randle and his group were the first ones to describe the relation between FFA in plasma and insulin resistance in skeletal muscle [71]. In 1967 Denton and Randle described lipid storage of in the rat gastrocnemius muscle [72]. The TAG content in skeletal muscle is increased in obesity [73,74]. The amount of the intramyocellular lipid in obese individuals is approximately 3–4% of total fibre area, whereas in the muscle of lean persons, this value decreases to 1–2 %. The dominating fatty acids in the skeletal muscle are palmitic and oleic acids, closely followed by linolenic acid [75]. Muscle TAG content has been shown to be positively correlated with serum TAG in diabetes subjects [76]. The skeletal muscle consist of approximately 0.25nmol DAG per mg tissue. DAG in

skeletal muscle has been shown to be upregulated in insulin resistance and type 2 –diabetes [12]. There is also a minor amount of cholesterol in the skeletal muscle [42].

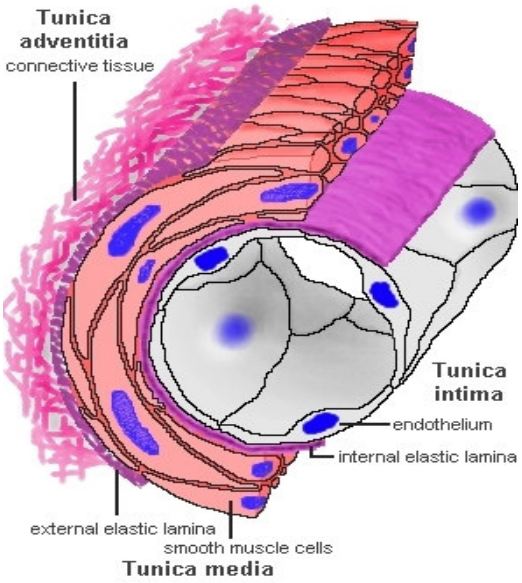

Figure 5 Illustration of the arortic divided in three different layer.
Tunica intima, tunica media and tunica adventita

The aortic wall

The structure

The aortic wall is divided into three layers, tunica intima, tunica media, and tunica adventitia. Tunica intima consists of a single layer of endothelial cells and some loose connective tissue, proteoglycans and the elastic lamina which separates the intima and the tunica media. The media consists of smooth muscle cells surrounded by elastic lamellae (e.g. collagen and elastine) and the tunica adventitia is composed of loose connective tissue layer with fibroblasts, collagen fibres, small blood vessels and nerves, and is the link between the artery and the surrounding tissue [77].

The lipid metabolism

The arterial wall is known to be metabolically active tissue with the capacity for lipid synthesis and possesses all necessary enzymes for this process. The supply of nutrients to the aortic wall goes via the luminal side [78]. Glucose is known to be the major substrate for the

arterial wall and endothelial cells have been shown to utilize exogenous glucose at physiological concentrations for their energy production [79]. Aortic endothelial cells do express insulin receptors with characteristics similar to those in other tissues, and GLUT1 is the major glucose-transporting protein in endothelial cells [80]. Further, the vascular smooth muscle cell utilizes primarily medium-chain fatty acids as substrate for energy [78]. TAG is synthesised from fatty acids and glucose is active in the arterial wall in response to insulin. They also express lipases that hydrolyse TAG in response to low insulin levels [81]. Elastic tissue has been shown to be important for the lipid accumulation in the aortic wall where it forms stable complex together with lipids [82]. Atherosclerosis is a cardiovascular disease related to intake of high fat diet and accumulation of lipids in the intima and media of the aortic wall.

Cholesterol

Different species response differently to cholesterol feeding, rat for example has been shown to have only a minor elevation of serum cholesterol levels, whereas in humans the plasma cholesterol level is increased moderate when fed with cholesterol-rich diet [83]. Plasma cholesterol is an important source of cholesterol in the aortic wall where it is transported with lipoprotein VLDL and LDL particles. The subendothelial retention of lipoproteins in the aortic wall is a key initiating process in atherogenesis [84]. The synthesies of cholesterol in the aortic wall has been demonstrated in several animals and humans [16,85]. Cholesterol homeostasis in the body is dependent on several factors, such as absorption, synthesis, storage, and excretion. The cholesterol concentration in humans and animals is at a constant level [86]. Cholesterol can be hydrolysed and excreted from the arterial wall [87] and is transported back to the liver by HDL-cholesterol proteins. The efflux of cholesterol from tissues goes via liver X receptors (LXR) situated in both macrophages, endothelial cells and smooth muscle cells [88,89]. LXRs operate as cholesterol sensors which protect from cholesterol overload [90].

Need of new methodology

Interests in studying lipid and metabolic disorders are expanding quickly. To cope with all these advances in disease research an imaging technique is. This has motivated to explore TOF-SIMS imaging techniques for further studies in lipid research, to discover lipids within biological tissues. Different methods have been used in the past. Electromicroscopy provides information about lipids in relation to organelles [91]. Histochemical staining with Oil Red O or Sudan dye is used to nonspecifically localize neutral lipids, while lipid-specific fluorescence probes are only available for cholesterol [92,93]. Chromatography methods previously used for lipid identification include gas chromatography, thin layer chromatography and high-performance liquid chromatography (HPLC). The separation of gangliosides for example was done by the use thin-layer chromatography and mass spectrometry [94,95]. HPLC separates TAG, DAG, acetates and even intact phospholipids by degree of unsaturation [96]. However, these techniques require extraction steps and lipid derivatization from tissues, which are both time-consuming and requires relatively large amounts of tissues and may result in lipid mobilization. Moreover, these techniques cannot reveal the heterogeneous distribution of lipids in the biological tissues. Different mass spectrometry (MS) techniques have been used in lipid research. For example, multiple precursor ions scanning hybrid quadrupole time of flight has been used very successfully in quantitative profiling of phospholipids [97]. Matrix enhanced SIMS (ME-SIMS) has been used for imaging phosphatidylcholine and sphingomyelin at cellular level [98] and Matrix-assisted laser desorption/ionization mass spectrometry (MALDI-MS) has been used for mass determination and distribution of phosphatidylcholine and cerebroside in rat brain [99]. MALDI-MS coupled with a time-of-flight technique leads to the acquisition of images with high mass resolution but relatively low spatial resolution, and the signal visibility is low, because of mass interference with matrix ion peaks [100]. Raman mapping and Fourier transform infrared (FTIR) imaging spectroscopy have been used for identifying polymorphism of ceramide [101]. However, these methods are lacking from chemical specificity.

Time of Flight Secondary Ion Spectrometry

TOF-SIMS ion microscope affords molecule-specific information without the incorporation of dye, isotopes or labels. Static TOF-SIMS is a surface-sensitive method where the primary ion dose is low, and thus provides molecular information of the sample surface with minor damage.The use of TOF-SIMS permits ion imaging in areas as large as 500 μm^2. Allow visualization of the morphology, topology, and chemical composition of significant peaks in the spectrum from the biologic samples with molecular weight of some thousand daltons. A recent modification is to use bismuth (Bi_3^+) cluster ion as the primary ion source, which increased spatial (100 nm) and mass (m/Δm 5000-10000) resolution [102] makes it possible, without any chemical pretreatment of the tissue, to measure directly the intensity of, and map, biomolecules within the tissues [103,104]. TOF-SIMS has several advantages. It has the possibility to direct compare signal intensity of different molecules in biological tissue and the ability to analyze sequential layers to form a three-dimensional analysis. Moreover, its detection of atomic concentrations can be as low as 10 ppm.

Historic

Secondary ion mass spectrometry (SIMS) is a relatively new technique for investigation in biological research. The first prototype to SIMS was developed by Castaing and Slodzian in the early 1960 in parallel to the Americans Liebel and Herzog [105]. There are two different operational regimes in SIMS, the dynamic and the static, which provides fundamentally different information. Dynamic SIMS, with a single non-pulsed primary beam is a rather destructive technique. The high numbers of bombarding ions allows depth profiling, reaching several microns with elemental sensitivity. The maximum mass range is typically ~ 250 m/z. The static SIMS appeared when Benninghoven (1970) reduced the primary ion current density on the sample [106]. It was first used to analyze inorganic compounds as oxids layers on metals, or mapping organic contaminats on semiconductors devices [107,108]. Static SIMS is surface mass spectrometric techniques which gives information about the chemical composition of the upper most monolayer of the bombarded surface with a high mass resolution. The technique creates some destruction of tissues and therefore it is necessary to use a very low dose of primary ions. Less than 1% of the top surface layer of atoms or molecules receives an ion impact [109]. Vickerman and his team saw the possibilities of static SIMS to be developed into a surface mass spectrometry in the middle of the 1970 [110], and from this technique, the TOF-SIMS instrument was developed. The first results were reported

by Chait and Standing in 1981 [111] by the implementation of TOF analyzers which achieved a significant improvement in mass resolution and transmission efficiency imaging [112-115]. Many interesting works have been done since the beginning of the 1980. For example 1981, Burns detected ions in the cat choroidea and in 1982, Na^+ and In^+ were detected in the kidney and cardiac tissue from rat [116]. The most famous one is the mapping of stable and radioactive isotopes in the thyroid gland by Berry et al in 1986 [117]. TOF-SIMS has also been used for drug detection in cells (anti-tumor drugs in histological sections) [118] to better evaluate successful early cancer treatments. Drug detection is accomplished indirectly by detecting a tag isotope naturally present or introduced by labeling, mainly with halogens,15N and 14C [118-120].

Imaging and detection of lipids with TOF-SIMS

Detection of lipids with TOF-SIMS was introduced by McMahon in 1995 by the imaging and detection of phosphatidylcholine and sphingomyeline in porcine brain and dog adrenal gland [121]. The same year Seedorf manages to detect cholesterol in blood from patients suffering from Smith-Lemli-Opitz syndrome [122], which is another example of early TOF-SIMS studies in the biomedical field. The technique is still developing mainly due to the development of new primary clustering sources as buckminister fulleren ($C60^+$), gold (Au^+) and bismuth (Bi^+). Its use in biological research is expanding. McQuaw et al have identified sphingomyelin in cholesterol domains in the process of raft formation in cellular membranes [123]. They have detected lateral heterogeneity of dipalmitoyl phosphatidylethanolamine-cholesterol in Langmuir-Blodgett film [124]. Using $Au3^+$ cluster ions Sjövall et al demonstrated cholesterol, sulfatides, phosphatidylinositols, and phosphatidylcholine [125]. Later on the $Bi3^+$ cluster ions have been used in the localization of cholesterol, phosphocholine and galactosylceramide in rat cerebellar cortex [126,127].

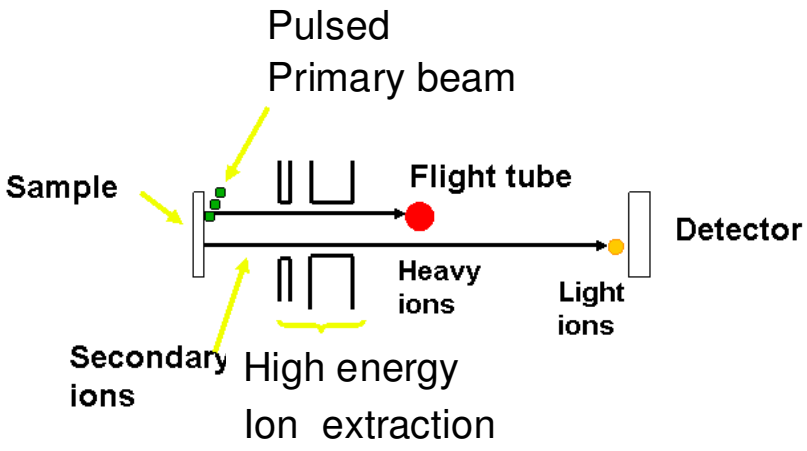

Figure 7 Schematic drawing of TOF-SIMS instrument

Principal of TOF-SIMS in biological samples

The "Time-of-Flight" of an ion is proportional to the square root of its mass, so that all different masses are separated during the flight and can be detected individually [128]. The sample is sputtered by a primary ion beam with energy between 5 and 25 keV. The beam can be pulsed with a puls lengt from ns up to µs. This generates a sort of collision cascade of atoms and molecules of the <3 upper most layer of the sample surface [129]. A cloud of atoms and molecules arises; most of them are neutrals only, some (approx. 1%) are ionized as secondary ions, positively or negatively charged [130]. The emitted ionized particles with different masses leave the surface at the same time via the deflection of the electron trajectories due to the Lorentz force which is transmitted into kinetic energy. Ions are separated charged by the TOF extraction optics. Ions are accelerated to a given energy with an electric potential and transferred into a field-free flight path of vacuum of approximately 2m. With a certain amount of kinetic and internal energy "they" are travelling in free and are separated by their mass in the end of the flight path the ionized particle hits a "detector" where the ions are detected and counted. The flight times of all the ions to the detector are electronically measured and related to the ion mass (m/z) [113,131]. Moreover, some of the identical secondary ions will leave the sample surface with different kinetic energy, which results in a decreased resolution due to a band broadening. To compensate for this, the instrument is equipped with a type of "mirror" called the reflectron in the end of the flight path. Ions with same mass-to-charge ratio but higher kinetic energy penetrate deeper into the reflector, delaying their time of arrival to the detector than the slower low-energy ions. This

process increases the resolution of the mass spectra [132]. Hence, for each primary ion pulse, a full mass spectrum is obtained. Thus a mass spectrum of all the ions is generated from the flight time spectrum. Every mass spectrum is transformed to one pixel in the image. One 256 x 256 pixel image contains 65.536 distinct mass spectra; each of them contains several hundreds of ion peaks.

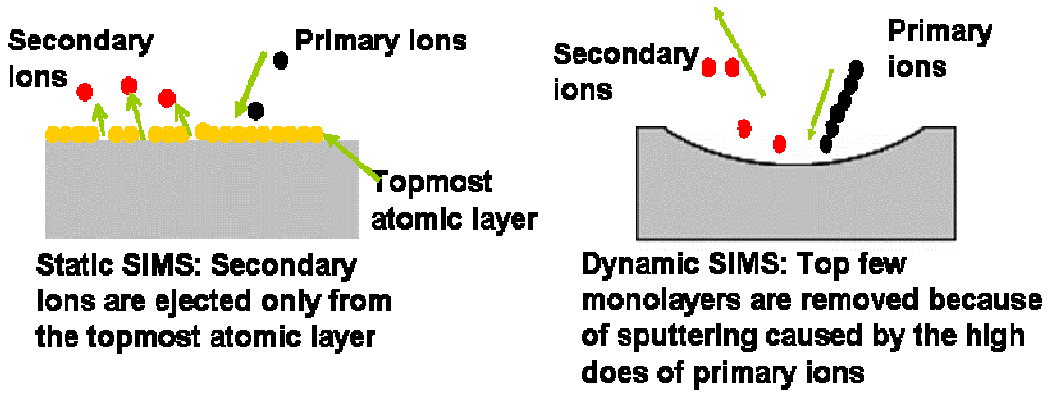

Figure 6 Illustration of the sputtering process with emissions of secondary ion

Primary ion source

The secondary ion yield depends to a large extend of the primary ion source. The basic types of ion guns for SIMS are the electron impact gas ion guns, surface ionization and liquid metal ion gun (LMIG). The electron impact gas ion gun operates with noble gases as argon (Ar^+), Xenon (Xe^+), oxygen (O^-, $O2^+$), $SF5^+$ ionized molecules and $C60^+$. These primary ion sources have been used mostly in dynamic SIMS that gives information about in-depth composition of the sample. Oxygen for example has been used in detection of positive ions such as magnesium (Mg^+) isotopes in the kidney [133]. The surface ionization source use Cesium (Cs^+) as the primary beam. Cs^+ produces a higher beam current and enhances the secondary ion yield, and it is mostly used for generating negative secondary ions [134,135] and as been used to localize isotopes in melanoma cells and tumour-infiltrating macrophages [136]. The LMIG uses liquid metals (at room temperature) as gallium (Ga^+), indium (In^+), Au^+, and Bi^+ as primary ion source. LMIG supplies a well focused ion beam. Ga^+ for example, offers high brightness and reasonable energy spread and has a lateral resolution of about 1 um. However, images obtained from tissue samples are generally limited to ions like the phosphatidylcholine headgroup of the membrane lipids at m/z 184 [126]. The major weakness of using

monoatomic primary ion sources, such as Ga^+, has been the low ion intensities and the high fragmentation of the high mass secondary ions.

A breakthrough with SIMS analysis resulted from the development of polyatomic cluster primary ion beam systems. Polyatomic ions involve the simultaneously collision of a number of atoms within a space of a few tenths of a nanometer. Because a cluster ion dissociates upon collision with a surface, the penetration depth of the elements of the cluster is reduced as compared to monoatomic primary ion bombardment [137,138]. This significantly increases the secondary ion yield and molecular specificity in the MS, even though the formation of oxide fragments arises with polyatomic ions [139]. The $Au3^+$ cluster ion beams for example have the potential to increase the secondary ion yield to 3 orders of magnitude compared to the conventional monoatomic Ga^+ [114]. By using $Au3^+$ Touboul detected cholesterol at m/z 385 in mouse brain [140] and later on different fatty acids and TAG in mouse leg [141]. The $Bi3^+$ cluster ions give better intensities and efficiencies of ions and produces less fragmentation of the parent ions and allow a better lateral and mass resolution[102,137,140,141]. The $C60^+$ is another used cluster ion source [142]. The $C60^+$ projectiles produce about a tenfold increase in the measured signal compared with Ga^+. However, this thin primary ion source is primarily used for depth-profiling generating 3-dimentional images [143].

Sputtering process for organic ion is not fully understood. The ion impact on the target is of major importance. During high energetic bombardment when the sample is receiving a high amount of energy, a crater can form. This often occurs when heavy ion such as Cu^+ or Au^+ cluster are used. When crater is formed only half of the sputtered atoms leave the surface, the other half is stocked in form of a crater rim [134]. Moreover, ionization of secondary ions can be formed either as ionization of the entire molecule M, through an ejection of an electron as radicals (M^+, M^-), by protonation $[M+H]^+$, de-proteonation $[M-H]^-$, or cationisation by Na^+, K^+ or Ag^+. The protonation (and de-protonation) or cationisation strongly depends on the matrix and this is referred as the matrix effect [144]. In principal the emission of secondary ions could be non-ionized in the absence of cations. On the contrary, adding Na^+ or K^+ salts to the sample the ionization of the analytes will occur. This was also shown in the presence of hydrogen-rich substrate [145]. To enhance the secondary ion yield other techniques can be used. For example, covering the sample by a nm-thick layer of gold or silver, has been shown to provide increased intensities for large analytes in biological tissue, so-called sample metallization (Meta-SIMS) [146].

Quantitative SIMS

Static SIMS produces qualitative information, but quantitative information is more complicated to obtain. However, even though TOF-SIMS is not being regarded as a quantitative technique, different quantitative approaches have been tried out with both static and dynamic TOF-SIMS. There are several factors that can influence the ion intensity in the sample, such as the chemical composition of the sample matrix, topography, matrix-and primary ion interactions, instrumental transmission, and detector response [114].
One approache to acheiving quantitative SIMS data was the implantation of an ion (e.g. isotope) of known concentration into the sample of interest [147,148]. By this approach the difficulty to control chemical environment can be compensated by simultaneously depositing an internal standard with the similar properties. The sample is then sputtered and depth profiled and the reference material signals are integrated over the sputtered time. The integrated ion intensity of the reference material can then be directly related to its known concentration, and a relative concentration of other elements can be calculated. This has been used in work by Harris et al [149] for quantifying the calcium distribution in biological samples. Moreover, this was also used for quantitative analysis of the immunosuppressive drug cyclosporine A (CsA), in whole blood of organ transplant patients. In this study, cyclosporine D, an analog of CsA which does not exhibit immunosuppressive activity, was used as an internal standard. Good correlation was obtained between HPLC, which is the specific method for the CSA analysis, and TOF-SIMS and MALDI results [150]. Another used approached is to add deuterium labeled molecules as internal standard. For example, direct quantification of cocaine in urine has been achieved by use of deuterated cocaine as an internal standard [151]. Analysis of L-DOPA is another example were a linear calibration curves were constructed by integrating the protonated molecular ion to silver ion peak area ratios over a known ion dosage and plotting versus the original sample concentration [152]. In addition, semi-quantitative information may be obtained by ToF-SIMS by normalizing the intensity of a signal of interest to a ubiquitous ion that produces a reasonably stable signal across samples of interest. This ion serves as an internal standard to account for variations in ionization efficiency across a sample caused by, for example, topographical and matrix effects [153]. This was applied in the work by Ostrowski where they relatively quantified cholesterol in membranes of individual cells from differt subjects [154]. These authors used a fatty acid fragment $C_5H_9^+$ as an internal standard to normalize the signal of interest. Relative quantitative approach is possible for tissue by using carbon (^{12}C) as an internal reference. This

approach was used for the quantification of halogens and calcium [155]. Standard preparation was determined based on molecular incorporation (halogens) or mixing (calcium) in methacrylate resin. Standard measurements were performed by depth analysis. Results obtained show that the relationship between the signal intensity measured and the elemental concentration is linear in the range of biological concentrations [155]. SIMS quantification has also been used to measure the concentration of ^{14}C –labeled molecules and their variabilities in different cells of human fibroblast. This procedure was assessed through local isotope $^{14}C/^{12}C$ ratio measurement. This relates the signal intensity of the labeled ^{14}C to that of the corresponding natural isotope (^{12}C) of known tissue concentration. Thus, differences in the concentration of arginine between different fibroblasts [156] could be obtained successfully.

Tissue preservation method

When preparing samples for TOF-SIMS analysis, several issues have to be taken into consideration. Preparation and fixation technique is very important to preserve the chemical and structural integrity of the tissue cells. Molecular species such as K^+, Ca^+, Na^+ as well as some proteins can diffuse, thus leading to incorrect results [113]. It is also necessary to avoid contaminations as they could hide native molecules in the sample surface. Most cells and tissue contain more than 70 % water. Given that samples are analyzed in ultra high vacuum, if they are placed in vacuum directly, artifacts will be created. Consequently, water must be removed from the sample. Before samples are analyzed by TOF-SIMS the ice must be eliminated by freeze-drying. In the freeze-drying process the pressure is lowered and vacuum created, adding heat to this low pressure environment allows the ice to sublimate into vapor. The removal of ice during the freeze-drying process can cause biomolecules to undergo significant structure changes. However, time, pressure and temperature in the freeze-drying process are factors that can be adjusted to avoid unnecessary mobilization of ions.

Cryo-sectioning can be immediately performed from liquid nitrogen (LN_2) snap-frozen samples. The cryo-sectioned sample can than be mounted directly on electrically conducted substrates and freeze-dried prior to SIMS analysis. The rapidity of the cooling process is another important issue. High speed freezing is vital to limit the ice-crystal size and related damage of the cells [119]. Another way is to use liquid propane for rapid freezing, which protects samples from ice-crystals without any prefixation or cryoprotectants, however this is very hazardous [157]. The newest method in freezing without cryo-protectants is the high-

pressure-freezing. High-pressure-freezing will immobilize all cells and/or tissue components immediately. This method is vitrifying the tissue fluids, i.e., absence of ice crystals, a so-called amorphos-ice. This technique reduces osmotic effects [158] and shifting and loss of ions in the sample [159] that occur with chemical fixation. High-pressure-freezing is at present the only way to vitrify or freeze well biological samples thicker than 50 µm [160]. Other methods have been tried out, for example the gluteraldyd fixation in protein film [161]. This has been shown to be successful in protein analysis.

Principal Component Analysis (PCA)

PCA is a common statistical technique for finding patterns in data of high dimension and expressing the data in such a way as to highlight their similarities and differences by transforming a number of (possibly) correlated variables into a (smaller) number of uncorrelated variables called principal components (PC). So, the first principal component accounts for as much of the variability in the data as possible, and each succeed component expresses for as much of the remaining variability as possible [162-164].

Data pre-processing

The pre-processing of the data before PCA analysis is important so it transforms the data into a format that will be more easily and effectively processed for the purpose of the user. There are a number of different tools and methods used for preprocessing; the most common ways are auto-scaling, mean-centering and normalization.

Auto scaling

Auto-scaling of the spectra are used to get a fair comparison between variables with an unequal spread. By auto scaling all variables, i.e. by dividing each peak values with the standard deviation of that peak are scaled so unit variance achieves. Auto-scaling allows all variables to influence equally.

Mean centering

If the variables have the same units, mean-centering may be the suitable option because that variables (peaks) with significantly variation are in fact more important, i.e. include more information regarding the spectra in the study, compared to those peaks with small variation. Mean centering consists of subtracting each peak with respectively peaks mean to achieve clarity in the model. The mean of the peaks will be equal to zero [165]. If you do not mean

center your data the first component does not really describe the largest direction of variation in the data, but rather it tends to describe the mean of the data, or at least some combination of the mean and the direction of largest variation.

Normalization

Normalization consists of dividing the spectra at each pixel by the total ion counts at that pixel. Normalization is typically done to reduce topographic or matrix effects.

Aim of the study

1) To test new technique “high-pressure frozen” for preserving tissues for TOF-SIMS analysis
2) To use imaging TOF-SIMS to localize different lipids in human adipose tissue and skeletal muscle.
3) To test whether multivariate analysis of TOF-SIMS spectra can be used for studying lipid changes:
    a) In the skeletal muscle, associated with obesity
    b) In the aorta, associated with high glucose intake

Methods and materials

Sample preparation

Human adipose tissue and skeletal muscle (paper I and II)

Healthy volunteers with a high body-mass index (age 14-16 yr, BMI>30, n=3) were used as subjects. A subcutaneous adipose tissue was obtained using the percutaneous needle biopsy technique with suction. A small piece of skeletal muscle was obtained after administration of local anaesthesia, by a Bergström needle (6 mm) from the middle part of lateral vastus muscle in the right leg. The biopsies were directly placed in ice-cold phosphate buffered saline (PBS; pH 7.4) until used for high-pressure freezing.

Rat aortic wall (paper III)

Aortas were taken from male Wistar rats with or without glucose drinking from birth to 6 months of age, directly placed into ice-cold phosphate buffered saline (PBS; pH 7.4) until used for high-pressure freezing, same procedures as described above.

High-pressure freezing and freeze-fracturing

An equal procedure was utilized using high-pressure freezing and freeze-fracturing in experiments of paper I, II and III. High-pressure-freezing was preformed at 2000 bar and -196°C using the EMPACT high pressure freezer (Leica, Vienna) as described in details by others [160]. Briefly, the sample is placed into a specimen holder composed of a gold carrier and a copper ring sealed on the top. The carrier is inserted into a pressure chamber through which the pressurized liquid nitrogen is jetted and the sample is quickly frozen. This procedure immobilizes cell components immediately. Samples were quickly transferred onto a pre-cooled copper block in a liquid nitrogen bath. With help of a pair of forceps, the copper ring was removed from the gold carrier to lay open a fractured surface. The sample on the carrier was transferred to a vacuum chamber and freeze-dried over night at 10^{-3} mbar. The freeze-dried tissues were kept in a desiccator under vacuum until TOF-SIMS measurements. The copper-rings were placed in a box filled with absolute ethanol and kept in -20°C until used.

Mouse skeletal muscle (paper IV)

Mice were anaesthetized with isofluran, and gastrocnemius skeletal muscle was extirpated and frozen immediately.

Cryo-sectioning

In paper IV cryo-sectioning was performed at -20 ºC with a Leica cryostat.
The frozen-tissue blocks were attached were taken from the -80 degree freezer and thawed in the cryostat machine for 45 min before the sample were sectioned. The sample was fastening with a sucrose solution on the tissue holder. Slices of 16 µm were cut, placed on an object slide and kept in the freezer at -20 ºC. Before measurement, the samples were freeze-dried in a vacuum chamber over night and directly analysed in vacuum by TOF-SIMS.

TOF-SIMS analysis

Measurements were performed using both an ION TOF TOF-SIMS IV and an ION TOF TOF-SIMS V instruments. Spectra of positive and negative ions were recorded using 25 keV Bi_3^+ primary ions and low-energy electron flooding for charge compensation as described previously [120]. To identify ion species present at respective surfaces the bunched mode was used. Spectra were recorded with the instrument optimized for maximum mass resolution (m/Δm = ≈3000–6000, beam diameter ≈5 µm, pulse width 10 ns, repetition rate 5 kHz) .The average primary ion current was 0.1 to 0.15 pA. Subsequently, high resolution secondary ion images (m/Δm 500, beam diameter ≈ 300 nm) were acquired in the burst alignment mode with a target current of 0.04 pA to 0.1 pA. Data were collected from several image fields on each section. The primary ion doses were kept well below the so-called static limit of 10^{13} ions/cm^2.

Pulse Mode

Two different modes have been used in imaging lipids in this thesis.

The bunched mode

The bunched mode means that ion pulses that LMIG bombard the surface with are bunched and in a short pulse (10-30 ns pulse). This mode provides a high mass-resolution (Δ/Δm 3000-6000) and a mass spectrum with thin peaks, but low lateral resolution (around 5 µm).

The burst alignment mode

The burst alignment mode means that the ion squirt is well-focused without the ability to compress the ion-pulses in time, thus primary ion bombardment occurs in a long pulse period. This mode provides high-lateral images (around 100 nm) however; the mass resolution is low ($m/\Delta m < 500$) and peaks are broader [115].

Charge compensation

TOF analysis depends on the sample being at its ground potential, otherwise the primary ion beam can be deflected by the sample charging and the secondary ions energies will be different [140] and their yield is reduced [112]. By irradiation of the surface with low energy electrons this is avoided. To handle this problem TOF-SIMS instrument is provided by an electron flood gun [113]. This function is activated during TOF-SIMS measurements.

Region of Interest analysis

Region of interest, abbreviated ROI, is imaging software tool. This is used to select specific regions within the image for particular purposes. ROI was used in paper I and IV. For defined regions (any shape and size) whitin the analysed area, it is possible to sum the mass spectra with the help of ROI at the entire pixel points within each defined region.

Morphology

The fractured copper rings that kept in ice-cooled ethanol 99% were transferred to propylene oxide and embedded in epoxy resin. Semi thin sections (about 0.8 µm thick) were cut with a Leica Ultracut R ultramicrotome, equipped with an FC 4E cryounit, collected on super frost glass and air-dried at room temperature. Tissue sections were stained with toluidine blue/azan. For visualization of slow twisted skeletal muscle fibres sections were incubated with monoclonal anti-skeletal myosin (slow) (1:100 dilution Sigma-Aldrich, St Louis, Missouri). A controlled corrosion of the section surface was obtained by etching the section for at least 15 min in sodium ethoxide diluted to 50 % with absolute ethanol and subsequently rehydrating in descending concentrations of ethanol. For histological analysis of lipids, 5 µm thick fresh frozen OCT imbedded skeletal muscle tissue sections were used and stained with oil-red. All histological stainings were analysed with microscopy automated software (KS400, Zeiss). To obtain information about tissue surface, the sample on the carrier that was used for TOF-

SIMS analysis was coated with palladium using an Edwards Xenosput 200 sputter. Scanning electron microscopy was performed using a Zeiss 982 Gemini.

Statistics

Variance patterns within the TOF-SIMS peak intensities were analysed by principal component analysis (PCA), described in detail elsewhere (10), using PLS_Toolbox 4.0 (Eigenvector Research, Wenatchee,WA) for MATLAB Version 7.1.0.246 R14 (The MathWorks Inc., Natick, MA). Spectral variations between samples are visualized in score plots, in which each dot represents an individual sample. The loadings plots show the contribution of each original variable (ion peak) to the new variables, principal components (PCs). All significant peaks with intensities above 50 count in the m/z region of 200-900 in the negative ion spectra and of 300-900 in the positive ion spectra were selected for analysis. Peak intensities were normalized to total ion intensities, and the data was auto-scaled before analysis. To further elucidate differences between two groups, the data were analyzed with Student's unpaired t test. Values are presented as means ± SD. A p-value less than 0.05 were considered statistically significant.

Summery of Results

Paper I

The most significant lipids found in human adipose tissue are palmitic acid (C16:0) at m/z 255, palmitoleic acid (16:1) at m/z 253, oleic (C18:1) at m/z 281 and stearic acid (18:0) at m/z 283. The phosphocholine head group at m/z 184, cholesterol at m/z 385, diacylglycerols in the m/z of (550 - 640) and triacylglycerols in the m/z (830 - 880) were also identified. The distribution of lipids in human adipose tissue was heterogeneous, with cholesterol localized in intracellular organelles and in the lipid droplets and FA/TAG localized in the lipid droplets. Thus, TOF-SIMS equipped with Bi_3^+ LMIG provides us an extra possibility to detect and localize different lipids in human adipose tissue at their original localization.

Paper II

This paper shows heterogeneous distribution of lipids in the human skeletal muscle. The most significant lipids found in human skeletal muscle are palmitic acid (C16:0) at m/z 255, palmitoleic acid (16:1) at m/z 253, oleic (C18:1) at m/z 281 and stearic acid (18:0) at m/z 283. The phosphocholine headgroup at m/z 184 representing phosphatidylcholine and sphingomyelin, cholesterol at m/z 385, diacylglycerols in the m/z (550 - 640) and triacylglycerol in the m/z (830 - 880) were also identified. The PC was mostly localized to the edge of the fibre, representing the sarcoplasma or endomysium. Cholesterol was weak, and more scattered in the edge of the muscle fibre. The fatty acids were scattered all over the fibre, more intensed in some area which could be related to the Type-1 skeletal muscle fibres. High DAG signal and low TAG signal were detected within the muscle fibre.

Paper III

In this paper multivariate analysis of TOF-SIMS spectra was used as a semi-quantitative tool for measuring lipids in the aortic wall. Rats were divided into two groups, with or without glucose in their drinking water from birth to 6 months of age. The results showed a statistically significant reduction in cholesterol ion intensity the aortic wall. The present study also showed that ratio of palmitoleic over palmitic acid (C16:1/C16:0) was increased and the ratio of linolenic over oleic acid (C18:2/C18:1) was decreased. The same pattern was shown for the ratios of DAGs with different fatty acid residues.

Paper IV

The results of Paper IV showed that there was an increased signal intensity of fatty acids and DAGs in skeletal muscle of the obese *ob/ob* mice. ROI showed that fatty acid signal intensities within the muscle cell were significantly increased in the ob/ob mice. These changes were revealed through, PCA analysis of TOF-SIMS spectra. TOF-SIMS images showed also increased fatty acids and DAGs in the skeletal muscle of the obese *ob/ob* mice when compared with the lean wild-type mice. Moreover, analysis of the ratio between different fatty acid peaks revealed changes in MUFA and PUFA that have been reported early in obesity. These changes in fatty acid composition were also reflected in the ratio between different DAGs and phosphatidylcholine that contain different fatty acid residues.

Results and Discussion

Tissue preserving method

The samples in papers I, II and III were preserved by high-pressure freezing, freeze-fracturing and freeze-drying. When samples are prepared by high-pressure freezing, all analytes in an intact cell are preserved at their original location [160]. TOF-SIMS is a surface-sensitive method, it is very important to avoid surface contamination which can hide native molecules in a tissue sample. In the freeze-fracturing process the sample is cracked into two parts generating two new fresh surfaces without contacting the preparation environment. One surface was used for TOF-SIMS imaging and another complementary surface was used for histological stainings. According to earlier studies, the fractured plane of a biological sample is irregular and extends along the inner hydrophobic area of the lipid bilayer in the plasma membrane or surfaces of organelles [166]. The irregular surface can lead to topographic effects that can present apparent enrichments or depletions of molecules, which have to be taken under consideration in the interpretation of images [167]. Although TOF-SIMS usually requires flat sample surfaces, rough surfaces can also be investigated [168]. However, care has to be taken when interpretating the data. Accordingly, both the human adipose tissue and skeletal muscle samples were freeze-fractured and were affected by topographic effects. Topographic effects will give significant effects on the yield of the secondary ions, e.g. band broadering and loss of signal intensities [134]. To compensate for topographic and/or matrix effects in rough samples, it is possible to divide the spectra at each pixel by the total ion counts at that pixel, so-called normalization. Another approach is to use principal component analysis where images are normalized against the first principal component [165]. However, normalization seems to result in loss of contrast and vividness in the image, so neither of these two normalization methods was applied for the images shown in this thesis.

Cryo-fix and cryo-sectioning

In paper IV, samples were plunge-frozen in liquid nitrogen and cryo-sectionized. The cryo-sectioning resulted in a smoother surface, thereby avoiding topographic affects in the sample (see fig 8a and b). Thus, less interference from topographic effects makes the semi-quantitative measurements of data more consistent. A drawback of cryo-sectioning is the possible ice-crystallization of water in the sample surface due to shift temperature. However,

ice-crystallization can be minimized if the tissue is cryofixed directly with a cryogen. We did not observe any influence of ice-cryztal formation, despite the fact that samples were untreated. To avoid water interfering in the mass spectra, a freeze-drying step in ultra-high vaacum before analysis is necessary [169]. This can cause ion motility and shrinkage of the sample. However, this step was used in both methods and for all of the samples. In addition, another disadvantage with the cryo-sectioning method is the possible ion redistribution when slicing the tissue [169].

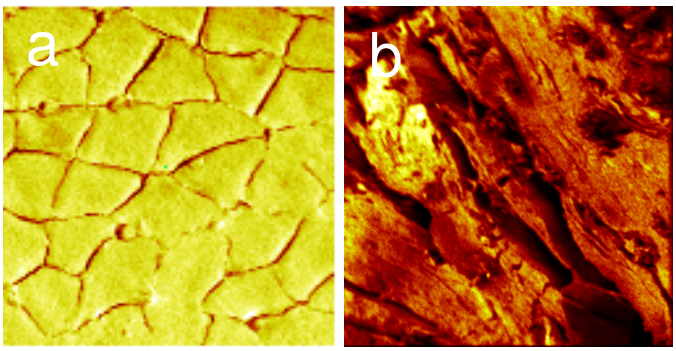

Figure 8 Total positively charged secondary ion TOF-SIMS images from cryofixated and cryosectionized mice skeletal muscle (a) and high-pressure-frozen and freeze-fractured human skeletal muscle (b).

Na^+ and K^+ ions are good markers for a successful fixation of the tissue. In an intact cell the K^+ ion concentrations are higher within the cell and Na^+ ions are higher in the extracellular compartments. If the cell is damaged, the membrane does not offer any barrier to ion gradients and the cell looses K and gain Na for equilibrium within the cells (see figure 9) [170].

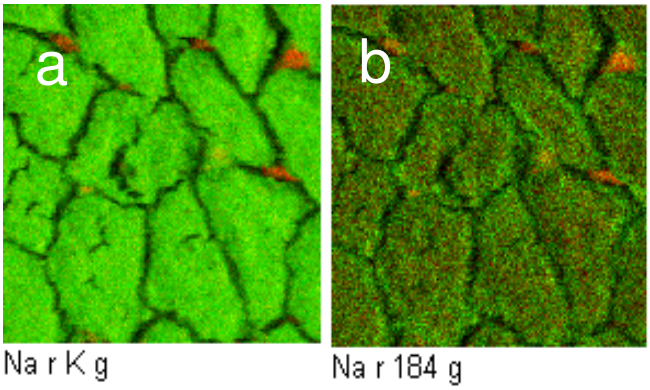

Figure 9 Illustrative images from mice skeletal muscle where in (a), Na^+ is visualized in extracellular compartments in red and K^+ in intracellular compartments in green. b), shows Na^+ in red, PC head group in green and merged signals in yellow

TOF-SIMS imaging of fat and muscle tissue

In papers I and II the TOF-SIMS technique was used to study lipid distribution in the human adipose tissue and skeletal muscle from obese youth. In paper I, high cholesterol signals were detected in the membrane of the adipocytes, a finding that is in agreement with previous results [56]. Other studies have shown that approximately 6% of the total cholesterol is located in the lipid droplets, in the form of cholesteryl esters [53]. Moreover, our data showed that clear-cut signals of DAG, fatty acids and low levels of TAG were located to the central part of the adipocyte. High CN signals derived from proteins and nucleic acids were found in structures related to loose connective tissue. The result of low TAG was unexpected, considering that lipids in the adipocyte contain 90-99 % of TAG. The reason for the low TAG signal is not clear. It might be that their high masses reduce their ability to reach high ion intensity. Another possible explanation is fragmentation of TAG. Indeed, in addition to TAG peak, we observed DAG peak in the TAG reference spectra. Fragmentation makes the lipid identification complex. However, fragmentation is also necessary to ensure the accuracy of lipid identities. The characteristic peak intensity ratio and "fingerprint patterns" are used to distinguish different compounds. The localization of fragments from one molecule may give us information of its possible relations to other fragments and their parent ions. For example, areas which exclusively express fatty acids or DAG without TAG indicates that fatty acids or DAG are naturally occurring molecules. Thirdly, low signal intensities of specific ions can also be caused by topographic features. Topographic effects could occur in the freeze-fractured sample surface as irregularities in the sample surface may affect the sputtering process of secondary ions. However, matrix effects caused by the high contribution of the secondary ions of K^+ and Na^+ localized to some areas in the sample are probably to some extent contributing to the shift in ion signals. These ions can either reduce the levels of other ion signals, the so-called quenching effect, or contribute to enhanced emission of some molecules. In cultured adipocytes, about 20-50 % of DAG is newly synthesized, however, less than 1% of DAG is accumulated in the adipocyte in vivo [171,172]. It has been shown that TAG synthesis, and/or lipolysis, may influence the accumulation of DAG in the adipose tissue [173]. In line with this, high DAG signals were observed in the adipose tissue, which probably arises from fragmented TAG as shown by reference spectra. Moreover, some of the DAG signals observed in the adipose tissue are probably unique localizations in the sample that are not related to TAG. High signals of fatty acids were also depicted in the adipose tissue. As the amount of non esterified fatty acids is low in the adipose tissue, it is probable that some of the

fatty acids emanated from fragmented TAG, DAG or PC. We observed that the most abundant fatty acids in adipose tissue, skeletal muscle and aortic wall were palmitic acid (C16:0) at m/z 255, and oleic acid (C18:1) at m/z 281. These are also the most frequent fatty acids in the circulation [174]. High levels of palmitic acid can lead to insulin resistance due to changes in the level of phosphorylation of the insulin receptor and insulin receptor substrate-1. Moreover, we identified linolenic acid (18:2) at m/z 279 a fatty acid that is used in the synthesis of prostaglandin. Low peaks at m/z 283 representing stearic acid (18:0) were identified from mass spectra of all tissues investigated in this thesis. Stearic acids are not so abundant in human tissues compared to palmitic acid (16:0) the incorporation into TAG and cholesterol is 30-40% lower while its incorporation into PC is 40% [27]. Accordingly, in mass spectra from human adipose tissue there were almost no TAG peaks found in the region of m/z 886-890 which are the peaks for TAG with stearic fatty acids incorporated in the fatty acid tails (see figure 11). The same pattern could be seen in the skeletal muscle, figure not shown.

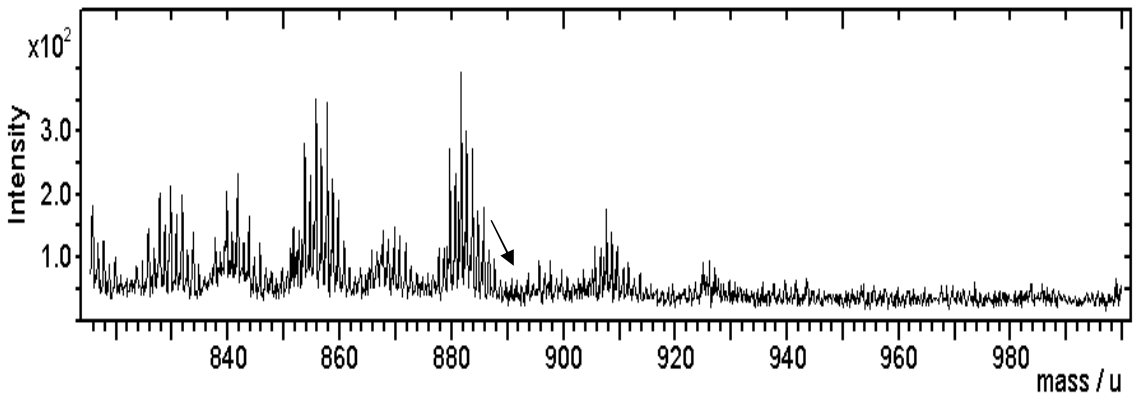

Figure 10 shows a spectrum from human adipose tissue in the range of m/z (800-1000)

Intake of an energy-rich diet will lead to obesity and lipid overloading in non-adipose tissues, so called ectopic tissues, in particular the insulin-sensitive skeletal muscle. In paper II TOF-SIMS was applied to image lipids in the skeletal muscle. Since ion microscopy is not a morphological tool, complementary techniques are generally needed for identification of microstructures in the SIMS image. In this study we have used scanning electron microscopy to identify morphology in areas where TOF-SIMS images were studied. Low TAG signals were detected in the skeletal muscle, probable due to the fact that the amount of lipid is generally much lower in the skeletal muscle than in adipose tissue. Moreover, TAG is likely to be fragmented in the same way in the skeletal muscle as in adipose tissue. Storage of

intramyocellular TAG in the skeletal muscle is associated with insulin resistance [175]. However, the primary cause of insulin resistance is not TAG, rather other intermediates of TAG like DAG, fatty acyl-CoAs or ceramide. DAG is known to activate protein kinase C (PKC). Site of PKC phosphorylates of serine/threonine residue on insulin receptor substrates, which inhibits insulin signalling [34]. Interestingly, high DAG signals in the m/z range 550-640 were detected in the skeletal muscle. The phosphocholine signals, on the other hand, were much more intense in the skeletal muscle than in the adipose tissue. This is probably due to the abundant sarcolemma and endomysium, which covers the skeletal muscle fibre. In addition, the skeletal muscle had low ion intensities of cholesterol. Accordingly, the cholesterol content in the skeletal muscle is only half that of the TAG content [154,155]. Endogenous cholesterol synthesis is low in the skeletal muscle and most cholesterol is transported from lipoproteins in the circulation [176].

We found that in the skeletal muscle, a highly complementary localization of fatty acids, DAGs and TAGs can be seen in the intracellular part of muscle cells, whereas PC and cholesterol are mostly located in the edge of the cells, probably in the plasma membrane e.g. sarcolemma. Low levels of cholesterol were scattered intracellularly in the fibre, possibly in the intracellular organelles such as the sarcoplasmic reticulum and the mitochondria. Earlier studies have shown that cholesterol is abundant in the lipid-laden caveolae of the sarcolemma [177]. Cholesterol is also found in the T-tubule and to a lesser amount in the sarcoplasmatic reticulum and mitochondria membrane [178]. The sarcolemma fluidity depends on the cholesterol content. Phosphatidylcholine is a major phospholipid found in the membrane of the sarcolemma, T-tubule and the sarcoplasmatic reticulum of the skeletal muscle cell [179]. We observed that the cholesterol-to-phospholipid ratio detected in the adipose tissue were 16 times higher than in the skeletal muscle.

Semi-quantitative comparation of TOF-SIMS spectra

In papers III and IV, static TOF-SIMS was used as a tool for semi-quantitative measurements of lipid alteration in tissues. To achieve this, we used principal component analysis (PCA) to reduce the data-set and to extract the most important information embedded in the data [115]. The 3-dimension score plot of the negative spectra in paper III showed that glucose-drinking rats could be distinguished from control rats on the PC2 and PC3 axes. The corresponding 3-dimension loading plot showed that linoleic acid (C18:2) was the main contributor to differences between the two groups. Further, the 3-dimension score plot of the positive spectra showed that the glucose-drinking rats could be distinguished from control rats

presumably on the PC2 and PC3 axes. The corresponding 3-d loading plot showed that the main contributor to this deployment was DAG and cholesterol. In addition, the ratios of different fatty acid peaks were calculated. Hereby, we found that the ratio of palmitoleic acid (C16:1) over palmitic acid (C16:0) was increased; while the ratio of linolenic acid (C18:2) over oleic acid (C18:1) was decreased. The same approached was used for DAG signals in positive spectra. We found the ratio of DAG with MUFA residues over DAG with SFA residues was upregulated. While, the ratio of DAG with PUFA residues over DAG with MUFA residues was significantly reduced in the glucose-drinking rats when compared with the control rats. This is in line with another study in sucrose-fed rats, where the proportion of MUFA were increased and PUFA was decreased [180].

In paper IV the same principal was used to explore lipid differences in skeletal muscles between the obese and lean mice. We observed increased signals in fatty acid and DAGs in the skeletal muscle from obese mice. Accordingly, increased fatty acid deposits in tissues of the *ob/ob* mice have been reported earlier [181-184]. The 3-dimensional score-plot from negative spectra of the skeletal muscle showed that the *ob/ob* mice could be distinguished from the lean wild-type mice mainly on the PC2 and PC3 axes. The corresponding loading-plot identified palmitoleic, oleic and linoleic acids as the main contributors to the cluster of the *ob/ob* mice. Furthermore, the 3-dimensional score-plot of the positive spectra from the skeletal muscle distinguished *ob/ob* mice from the wild-type mice, mainly on the PC2 and PC3 axis. The corresponding loading-plot showed that the main contributors were DAGs and cholesterol. The ratio between different fatty acids showed that the proportion of palmitoleic acids and oleic acids was upregulated while the proportion of linoleic acid was decreased in the *ob/ob* mice as compared to the lean mice. This is in line with changes in MUFAs and PUFAs that have been reported earlier in obesity [181,183]. These changes in fatty acid composition were also reflected in the ratio between different DAGs and phosphatidylcholine that contain different fatty acid residues as shown in our study. Moreover, it has been shown that increased MUFA concentrations in muscle phospholipids are positively correlated with fasting insulin concentrations and insulin resistance [185,186]. One of the reasons for the accumulation of MUFA is the activation of the enzyme stearoyl-CoA desaturase (SCD-1) associated with obesity. SCD-1 is rate limiting enzyme catalysing the synthesis of MUFA, mainly oleic and palmitoleic acids, which are major component in tissue lipids [187].

Further, we observed that arachidonic acid (C20:4) over dihomo-gamma-linolenic acids (DGLA, C20:3) were upregulated, while DGLA over linoleic acids decreased in the obese ob/ob mice. The increased C20:4/C20:3 ratios and its relation to obesity and insulin resistance are controversial since both increment and decrement have been reported in obese subjects [17,188].

Moreover, region-of-interest analysis showed that fatty acid signal intensities within the muscle cell were statistically significantly increased in *ob/ob* mice compared with the lean wild-type mice. The increased DAG may contribute to insulin resistance through the activation of protein kinase C family [12]. Moreover, insulin resistance is characterized by a specific fatty acid pattern in the serum lipid esters, as well as in lipid storage and in cell membranes of the skeletal muscle. TOF-SIMS overlay images showed that palmitic and oleic acids were located within the same muscle fibre, whereas stearic acid seemed to be located in other fibres (see figure 11). It is known that the lipid content is higher in oxidative type-1 fibres than in type-2 skeletal muscle fibres. Oxidation of stearic acid has been shown to be significantly less than that of oleic acid in both the fed and fasted states [189]. By this background it is possible that palmitoleic and oleic are located to the oxidative type-1 fibres whereas stearic acid is located to type-2 fibres.

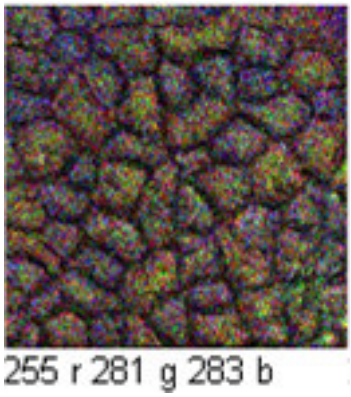

Figure 11 shows TOF-SIMS image of a cryofixed and cryosectionized skeletal muscle sample from an ob/ob mouse. The different fatty acid distribution is shown whitin the skeletal muscle fibre in different colour according to their distribution. Palmitic acid at m/z 255 is shown in red colour, oleic acid at m/z 281 shown in green and stearic acid at m/z 283 shown in blue colour

However, some technical details about TOF-SIMS and its influence on quantification are needed to be taken in consideration when quantification approaches is performed. First, the absolute ion yield in a sample depends on the surrounding molecules, their chemical binding and the type of environment to which they are associated. Cationization of molecular ions

with Na^+ and K^+ may for example influence the ion yield of a specific ion. Na^+ is known for cationisation with ceramides, and the presence of water in the sample surface will increase ion intensity of phosphocholine [190]. This so-called matrix effect is a known phenomenon in TOF-SIMS methodology [191]. Thus, when quantifying with TOF-SIMS data, the matrix effect has to be taken into consideration. TOF-SIMS has been shown to be useful in quantifying cyclosporine A in blood samples [192] and cocaine has been successfully measured by TOF-SIMS in urine [151]. In these studies, known concentration of internal standards was added to the sample, and by calibration curves, it was possible to determine the concentration of the analytes of interest in the sample. However, this approach is very difficult to apply on tissue as it is difficult to add internal standard to the tissue as it would hide native molecules. Moreover, the concentration of analyte molecules at the very surface must be known and typically we only know the bulk concentration of a reference sample. Instead, using appropriate control group offers the possibility for comparing analytes from the same type of tissue in different groups. When quantitatively comparing samples from similar areas in the same type of tissue (matrix), the matrix effect should be similar from one sample to the other, and the secondary ion yields are likely to be similar. Variations in other parameters, such as the surface inclination, acquisition time, primary ion source and current, the angle of the beam and charge state of the matrix, should also be the same [135,193]. Thus, it is also possible to calculate the ratio of different peaks within the same sample and to compare the ratios between different groups. With this approach we identified differences in the fatty acid composition as a result of obesity and high glucose intake.

High-carbohydrate diet and lipid accumulation in the aortic wall

It has been shown that a high-carbohydrate diet contributes to obesity with raised TAG and reduced HDL content in blood plasma [194]. Accordingly, we found that rats with a high-glucose intake had both an increased plasma TAG and a reduced HDL-cholesterol level. Lowering of the HDL-cholesterol level plays an important role in endothelial activation and accumulation of cholesteryl esters in the aortic wall [195,196]. However, our study showed decreased cholesterol signals in the aortic wall. Despite the reduced HDL-cholesterol in the glucose-drinking rats, the level of LDL-cholesterol and total cholesterol remained unchanged. It has shown that high-carbohydrate diet reduce blood levels of both HDL- and LDL-

cholesterol plasma levels [197]. It is possible that both reduced HDL-and raised LDL-cholesterol plasma levels are required for cholesterol accumulation in the aortic wall.

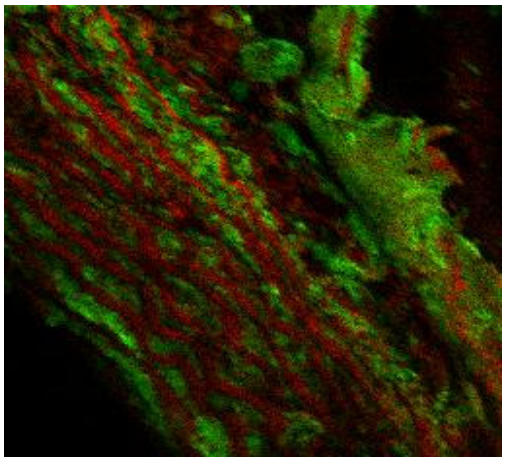

Figure 12 shows the TOF-SIMS image of the rat aotic wall where cholesterol is shown in red colour, mainly located to the lamella regions and the PC is shown in green colour which surround the cholesterol signals.

It has shown that rats fed a high-fat diet had reduced body weights, and volume and number of adipocytes compared to rats receiving a high-carbohydrate diet. Even though rats fed a high carbohydrate diet gained more fat the lipolytic activity in the aortic wall was not reduced, while this occurred in rats fed with high-fat diet. In addition rats fed with high-fat diets had also a higher lipid disposition in the aortic wall than rats fed with high-carbohydrate diet [198]. Moreover, rats receiving diet high in saturated fat for 15 months had no vascular changes in coronary arteries or aorta despite significant differences in plasma triglyceride and cholesterol levels [199]. Thus, high-carbohydrate diet does not necessarily lead to lipid accumulation in the aortic wall. Accordingly, we showed that high glucose intake in rat did not lead to more intensed lipid signals in the aortic wall. In contrast, glucose-drinking led to decreased cholesterol ions signals in the aortic wall.

The association between increased plasma triglyceride-rich lipoproteins and a high lipid accumulation within the aortic wall is complex. Metabolic disorder resulting in severe increase in triglyceride-rich lipoproteins, such as lipoprotein lipase deficiency, is not associated with an increased risk of atherosclerosis. In these disorders, lipoproteins are of such size that they cannot enter the aortic wall and thus do not directly promote atherogenesis [200,201]. Lipoproteins primarily carry two type's lipids: cholesterol and TAG. However, these two lipids have different fats. TAG is mainly transported into adipose tissue and skeletal

muscle where the fatty acids are stored or oxidized for energy production. Cholesterol is continuously transported between the liver, intestines and other extrahepatic tissues. Cholesterol serves as a structural component of the cellular membrane and as a precursor to the synthesis of steroid hormones and bile acids [86].

The liver X receptors (LXRs) are involved in lipid metabolism and reverse cholesterol transport, glucose has been shown to be an LXR agonist and upregulated in the expression of the LXR gene [90]. LXRs are expressed in endothelial cells [88] and in human coronary artery vascular smooth muscle cells [89]. LXR stimulates cholesterol efflux to lipid-poor apolipoproteins [202]. It is possible that high-glucose intake can activate LXRs in the aortic wall and this pathway may explain the decreased cholesterol in the rat aorta.

Moreover, we observed that rats receiving high glucose intake had a major reduction of pellets consumption, probably due to the high energy intake of glucose reducing their hunger, which has been seen in other studies [203]. This means that their protein intake was lowered during six months of life. Interestingly, a low-protein diet during neonatal and postnatal life has been shown to reduce arterial wall thickness and elastic tissue [204]. The reduction in protein intake during neonatal and postnatal life probably contributed to the reduction of cholesterol in the aortic wall. It has been shown that elastic tissue is important for the accumulation of lipids in the aortic wall, as elastine forms stable complex together with cholesterol [82]. TOF-SIMS images of rat aorta showed that cholesterol and oxysterols are located to the elastic lamellae in the aortic wall [205] (see figure 12). Furthermore, correlation between collagen synthesis and cholesterol has been shown [206]. Moreover, high-pressure freezing has been shown to retain relationships between cells, collagen and elasin in the aortic media [207]. Thereby, this would be adequate method of preserve samples for semi-quantitative measurement of lipids in the aortic. Thus, it is possible that the decreased cholesterol signals in the aortic wall are caused by protein deficiency during neo- and postnatal life due to high glucose consumption. Reduced HDL-cholesterol levels in the blood lead to augmented cholesterol concentration primarily in the adipose tissue, which is our body's largest cholesterol storage compartment [51]. Moreover, it has been shown that cholesterol depletion in the endothelial cell increases the stiffness of the membrane by altering the properties of the submembrane F-actin and/or its attachment to the membrane [208].

Conclusions

This thesis showed the possibility of using TOF-SIMS in tissue research. Peaks from fatty acid, DAG, TAG cholesterol and phosphatidylcholin were identified in the TOF-SIMS spectrum, from the skeletal muscle, adipose tissue and aortic wall, tissues which are connected to insulin resistance and metabolic syndrome. This thesis is also revealing a semi-quantitative way of using TOF-SIMS for comparation of lipids in the aortic wall and in the samples of mouse skeletal muscle. By principal component analysis we were able to reveal changes of lipids in the samples between experimental and control groups. This revealed interesting data with the use of unfixed samples. TOF-SIMS is an interesting technique of mapping lipids in biological tissues and future experiment with this technique should improve the knowledge of lipids interaction in metabolic diseases and cellular processes.

Acknowledgement

Jag vill uttrycka min tacksamhet till alla Er som medverkat till att denna avhandling blivit klar

Jag vill tacka

Min handledare Professor Peter Friberg, för vägledning och stöd i arbetet

Min bihandledare Docent Yun Chen för att du tålmodigt och glatt väglett mig i detta arbete och att du alltid, alltid tar Dig tid till att förklara oförståeliga saker och på ett lättbegriplig sätt och för Du så generöst delar med Dig av din kunskap.

Peter Sjövall and Jakob Malm, SP i Borås, för all hjälp med TOF-SIMS

Övriga medlemmar i Peter Friberg grupp: Marika för din hjälpsamhet med administrativa frågor, Gun och Frida

Ulla Gustavsson-Weicer för all hjälp i den tidigare gruppen

Heimir, för all hjälp med alla tänkbara data tekniska problem

Merja Meuronen Österholm, Christina, Mutjaba Siddiqui och Magnus Gustavsson för att Ni skapade/skapar en trevlig atmosfär på Wlab.

Christina Ericsson medicinska institutionen för stöd

Rosie Perkins för hjälp med korrekturläsning av manus

Anna H för hjälp med bildbehandling o Birgitta O för gott sammarbete när vi delade lab.

Till alla i ”skrivarrummet” för att ni alltid är trevliga och bussiga när man frågar om hjälp:

Sara Sjöberg, tack för alltid uppmuntrande ord och trevliga pratstunder

Liliana för trevligt sällskap i skrivarrummet

Levent Akurek för ditt engagemang med torsdagseminarierna samt tidigare ”journalclub”

Alla Ni andra forskare på Wlab som bidrar till en trevlig atmosfär att forska i.

Fei Tian, vi som följt åt nu i många år, tack för gott sammarbete under denna tid, stöd samt trevliga pratstunder. Det kommer att kännas tomt nu.

Kristina Nilsson för fin vänskap.

Mina kära vänner: Karin, Sara Annette, Sanna och Katta, tack för alla roliga stunder och minnen tillsammans.

Moster Ronny för att Du alltid kommer ihåg oss.

Mina syskon Filip, Dag och Sofia med familjer … Vad vore livet utan syskon… Roligt att vi hamnat i Göteborg igen allihop.

Till mamma i minne för all trygghet och uppbackning

Bernard, för att du fick mig att tro att det var möjligt och allt som förgyller vardagen

Ylva

References

[1] Bansilal, S., Farkouh, M.E. and Fuster, V. (2007) Am J Cardiol 99, 6B-14B.
[2] Keller, K.B. and Lemberg, L. (2003) Am J Crit Care 12, 167-70.
[3] Goran, M.I., Ball, G.D. and Cruz, M.L. (2003) J Clin Endocrinol Metab 88, 1417-27.
[4] Steinberger, J. and Daniels, S.R. (2003) Circulation 107, 1448-53.
[5] De Meyts, P. (2004) Bioessays 26, 1351-62.
[6] Krentz, A.J. (1996) Bmj 313, 1385-9.
[7] Greenfield, J.R. and Campbell, L.V. (2004) Clin Dermatol 22, 289-95.
[8] Abate, N., Garg, A., Peshock, R.M., Stray-Gundersen, J. and Grundy, S.M. (1995) J Clin Invest 96, 88-98.
[9] Garg, A. (2006) Clin Cornerstone 8 Suppl 4, S7-S13.
[10] Delarue, J. and Magnan, C. (2007) Curr Opin Clin Nutr Metab Care 10, 142-8.
[11] Hegarty, B.D., Furler, S.M., Ye, J., Cooney, G.J. and Kraegen, E.W. (2003) Acta Physiol Scand 178, 373-83.
[12] Schmitz-Peiffer, C. (2002) Ann N Y Acad Sci 967, 146-57.
[13] Kelley, D.E. and Mandarino, L.J. (2000) Diabetes 49, 677-83.
[14] Goodpaster, B.H., He, J., Watkins, S. and Kelley, D.E. (2001) J Clin Endocrinol Metab 86, 5755-61.
[15] Goodpaster, B.H. and Kelley, D.E. (2002) Curr Diab Rep 2, 216-22.
[16] Vance, V.a. (2002), Vol. 35.
[17] Decsi, T., Csabi, G., Torok, K., Erhardt, E., Minda, H., Burus, I., Molnar, S. and Molnar, D. (2000) Lipids 35, 1179-84.
[18] Quastel, J.H. (1967) Science 158, 146-61.
[19] Yeagle, P.l.
[20] Garg, M.L. and Sabine, J.R. (1988) Biochem J 251, 11-6.
[21] Hulbert, A.J., Turner, N., Storlien, L.H. and Else, P.L. (2005) Biol Rev Camb Philos Soc 80, 155-69.
[22] Emken, E.A. (1994) Am J Clin Nutr 60, 1023S-1028S.
[23] Huitema, K., van den Dikkenberg, J., Brouwers, J.F. and Holthuis, J.C. (2004) Embo J 23, 33-44.
[24] Lands, W.E. and Hart, P. (1965) J Biol Chem 240, 1905-11.
[25] Lee, D.P., Deonarine, A.S., Kienetz, M., Zhu, Q., Skrzypczak, M., Chan, M. and Choy, P.C. (2001) J Lipid Res 42, 1979-86.
[26] Coleman, R.A. and Haynes, E.B. (1985) Biochim Biophys Acta 834, 180-7.
[27] Besterman, J.M., Duronio, V. and Cuatrecasas, P. (1986) Proc Natl Acad Sci U S A 83, 6785-9.
[28] Schmitz-Peiffer, C., Browne, C.L., Oakes, N.D., Watkinson, A., Chisholm, D.J., Kraegen, E.W. and Biden, T.J. (1997) Diabetes 46, 169-78.
[29] Bruce, C. and Tall, A.R. (1995) Curr Opin Lipidol 6, 306-11.
[30] Simons, K. and Ikonen, E. (1997) Nature 387, 569-72.
[31] Pike, L.J. (2004) Biochem J 378, 281-92.
[32] Xi, Z.P. and Wang, J.Y. (2003) J Nutr Sci Vitaminol (Tokyo) 49, 210-3.
[33] Jakobsson, A., Westerberg, R. and Jacobsson, A. (2006) Prog Lipid Res 45, 237-49.
[34] Seubert, W. and Podack, E.R. (1973) Mol Cell Biochem 1, 29-40.
[35] Nakamura, M.T. and Nara, T.Y. (2004) Annu Rev Nutr 24, 345-76.
[36] Parker-Barnes, J.M., Das, T., Bobik, E., Leonard, A.E., Thurmond, J.M., Chaung, L.T., Huang, Y.S. and Mukerji, P. (2000) Proc Natl Acad Sci U S A 97, 8284-9.

[37] Vessby, B., Gustafsson, I.B., Tengblad, S., Boberg, M. and Andersson, A. (2002) Ann N Y Acad Sci 967, 183-95.
[38] Shaw, H.B. (1901) J Anat Physiol 36, 1-13.
[39] Mirski, A. (1942) Biochem J 36, 232-41.
[40] Renold, A.E. and Marble, A. (1950) J Biol Chem 185, 367-75.
[41] Haugaard, N. and Marsh, J.B. (1952) J Biol Chem 194, 33-40.
[42] Del Vecchio, A., Keys, A. and Anderson, J.T. (1955) Proc Soc Exp Biol Med 90, 449-51.
[43] Rabinowitz, D. and Zierler, K.L. (1962) J Clin Invest 41, 2173-81.
[44] Imaichi, K., Fukuda, J.I., Oyama, K. and Mukawa, A. (1965) J Biochem (Tokyo) 58, 463-9.
[45] Siiteri, P.K. (1987) Am J Clin Nutr 45, 277-82.
[46] Zhang, Y., Proenca, R., Maffei, M., Barone, M., Leopold, L. and Friedman, J.M. (1994) Nature 372, 425-32.
[47] Kershaw, E.E. and Flier, J.S. (2004) J Clin Endocrinol Metab 89, 2548-56.
[48] Murphy, D.J. (2001) Prog Lipid Res 40, 325-438.
[49] Martin, S. and Parton, R.G. (2006) Nat Rev Mol Cell Biol 7, 373-8.
[50] Galton, D.J. and Wilson, J.P. (1970) Clin Sci 38, 649-60.
[51] Krause, B.R. and Hartman, A.D. (1984) J Lipid Res 25, 97-110.
[52] Prattes, S., Horl, G., Hammer, A., Blaschitz, A., Graier, W.F., Sattler, W., Zechner, R. and Steyrer, E. (2000) J Cell Sci 113 (Pt 17), 2977-89.
[53] Schreibman, P.H. and Dell, R.B. (1975) J Clin Invest 55, 986-93.
[54] Schiaffino, S. and Reggiani, C. (1996) Physiol Rev 76, 371-423.
[55] Hess, A. (1970) Physiol Rev 50, 40-62.
[56] Le Lay, S., Ferre, P. and Dugail, I. (2004) Biochem Soc Trans 32, 103-6.
[57] Tauchi-Sato, K., Ozeki, S., Houjou, T., Taguchi, R. and Fujimoto, T. (2002) J Biol Chem 277, 44507-12.
[58] Kovanen, P.T., Nikkila, E.A. and Miettinen, T.A. (1975) J Lipid Res 16, 211-23.
[59] Zweytick, D., Athenstaedt, K. and Daum, G. (2000) Biochim Biophys Acta 1469, 101-20.
[60] Pol, A., Martin, S., Fernandez, M.A., Ferguson, C., Carozzi, A., Luetterforst, R., Enrich, C. and Parton, R.G. (2004) Mol Biol Cell 15, 99-110.
[61] Blanchette-Mackie, E.J. et al. (1995) J Lipid Res 36, 1211-26.
[62] Bostrom, P., Rutberg, M., Ericsson, J., Holmdahl, P., Andersson, L., Frohman, M.A., Boren, J. and Olofsson, S.O. (2005) Arterioscler Thromb Vasc Biol 25, 1945-51.
[63] Spector, A.A. (1984) Clin Physiol Biochem 2, 123-34.
[64] Merkel, M., Eckel, R.H. and Goldberg, I.J. (2002) J Lipid Res 43, 1997-2006.
[65] Swierczynski, J., Zabrocka, L., Goyke, E., Raczynska, S., Adamonis, W. and Sledzinski, Z. (2003) Mol Cell Biochem 254, 55-9.
[66] Holm, C. (2003) Biochem Soc Trans 31, 1120-4.
[67] Brooke, M.H. and Kaiser, K.K. (1970) Arch Neurol 23, 369-79.
[68] Schrauwen-Hinderling, V.B., Hesselink, M.K., Schrauwen, P. and Kooi, M.E. (2006) Obesity (Silver Spring) 14, 357-67.
[69] Wertheimer, E. and Ben-Tor, V. (1952) Biochem J 50, 573-6.
[70] Andersson, A., Sjodin, A., Hedman, A., Olsson, R. and Vessby, B. (2000) Am J Physiol Endocrinol Metab 279, E744-51.
[71] Arslanian, S.A. and Kalhan, S.C. (1994) Diabetes 43, 908-14.
[72] Denton, R.M. and Randle, P.J. (1967) Biochem J 104, 416-22.
[73] Pagliassotti, M.J., Pan, D., Prach, P., Koppenhafer, T., Storlien, L. and Hill, J.O. (1995) Obes Res 3, 459-64.

[74] Pan, D.A., Lillioja, S., Kriketos, A.D., Milner, M.R., Baur, L.A., Bogardus, C., Jenkins, A.B. and Storlien, L.H. (1997) Diabetes 46, 983-8.
[75] Thomas, T.R., Londeree, B.R., Gerhardt, K.O. and Gehrke, C.W. (1978) Mech Ageing Dev 8, 429-34.
[76] Standl, E., Lotz, N., Dexel, T., Janka, H.U. and Kolb, H.J. (1980) Diabetologia 18, 463-9.
[77] Stout, R.W. (1976) Acta Diabetol Lat 13, 87-92.
[78] Odessey, R. and Chace, K.V. (1982) Am J Physiol 243, H128-32.
[79] Krutzfeldt, A., Spahr, R., Mertens, S., Siegmund, B. and Piper, H.M. (1990) J Mol Cell Cardiol 22, 1393-404.
[80] Bar, R.S., Boes, M., Dake, B.L., Booth, B.A., Henley, S.A. and Sandra, A. (1988) Am J Med 85, 59-70.
[81] Stein, Y., Stein, O. and Shapiro, B. (1963) Biochim Biophys Acta 70, 33-42.
[82] Jacotot, B., Beaumont, J.L., Monnier, G., Szigeti, M., Robert, B. and Robert, L. (1973) Nutr Metab 15, 46-58.
[83] Lin, D.S. and Connor, W.E. (1980) J Lipid Res 21, 1042-52.
[84] Tabas, I., Williams, K.J. and Boren, J. (2007) Circulation 116, 1832-44.
[85] Dayton, S. (1959) Circ Res 7, 468-75.
[86] Bhattacharyya, A.K. (1989) Artery 16, 84-9.
[87] Eriksson, M., Carlson, L.A., Miettinen, T.A. and Angelin, B. (1999) Circulation 100, 594-8.
[88] Norata, G.D., Ongari, M., Uboldi, P., Pellegatta, F. and Catapano, A.L. (2005) Int J Mol Med 16, 717-22.
[89] Blaschke, F. et al. (2004) Circ Res 95, e110-23.
[90] Mitro, N., Mak, P.A., Vargas, L., Godio, C., Hampton, E., Molteni, V., Kreusch, A. and Saez, E. (2007) Nature 445, 219-23.
[91] Hoppeler, H. (1986) Int J Sports Med 7, 187-204.
[92] Molotkovsky, J.G., Manevich, Y.M., Gerasimova, E.N., Molotkovskaya, I.M., Polessky, V.A. and Bergelson, L.D. (1982) Eur J Biochem 122, 573-9.
[93] Bergelson, L.D., Molotkovsky, J.G. and Manevich, Y.M. (1985) Chem Phys Lipids 37, 165-95.
[94] Svennerholm, L., Bruce, A., Mansson, J.E., Rynmark, B.M. and Vanier, M.T. (1972) Biochim Biophys Acta 280, 626-36.
[95] Holm, M., Mansson, J.E., Vanier, M.T. and Svennerholm, L. (1972) Biochim Biophys Acta 280, 356-64.
[96] Markello, T.C., Guo, J. and Gahl, W.A. (1991) Anal Biochem 198, 368-74.
[97] Ekroos, K., Chernushevich, I.V., Simons, K. and Shevchenko, A. (2002) Anal Chem 74, 941-9.
[98] Altelaar, A.F., Klinkert, I., Jalink, K., de Lange, R.P., Adan, R.A., Heeren, R.M. and Piersma, S.R. (2006) Anal Chem 78, 734-42.
[99] Jackson, S.N., Ugarov, M., Egan, T., Post, J.D., Langlais, D., Albert Schultz, J. and Woods, A.S. (2007) J Mass Spectrom 42, 1093-8.
[100] Schwartz, S.A., Reyzer, M.L. and Caprioli, R.M. (2003) J Mass Spectrom 38, 699-708.
[101] Raudenkolb, S., Wartewig, S. and Neubert, R.H. (2003) Chem Phys Lipids 124, 89-101.
[102] Touboul, D., Kollmer, F., Niehuis, E., Brunelle, A. and Laprevote, O. (2005) J Am Soc Mass Spectrom 16, 1608-18.
[103] Tahallah, N., Brunelle, A., De La Porte, S. and Laprevote, O. (2008) J Lipid Res 49, 438-54.

[104] Malmberg, P., Nygren, H., Richter, K., Chen, Y., Dangardt, F., Friberg, P. and Magnusson, Y. (2007) Microsc Res Tech 70, 828-35.
[105] R Castaing, G.S. (1962) J.microscope 1, 395-410.
[106] Benninghoven (1970) Z Physik 230, 417-30.
[107] Benninghoven, A. (1971) Surface Science 28, 541-562.
[108] Benninghoven, A. (1973) Surface science 35, 427-457.
[109] Benninghoven, A. (1994) Surface science 299-300, 246-260.
[110] John C Vickerman, A.B.a.N.M.R. (1989) in: Secondary Ion Mass Specrtrometry Principles and Applications, pp. 1-8.
[111] Chait BT, S.K. (1981) International Journal of Mass Spectrometry and Ion Physics 40, 185-193.
[112] Belu, A.M., Graham, D.J. and Castner, D.G. (2003) Biomaterials 24, 3635-53.
[113] Vickerman, J.C. (2001) in: TOF-SIMS surface analysis by mass spectrometry, pp. 1-40.
[114] Pacholski, M.L. and Winograd, N. (1999) Chem Rev 99, 2977-3006.
[115] Sodhi, R.N. (2004) Analyst 129, 483-7.
[116] Burns, M. (1981) Anal Chem 53, 2149-2152.
[117] Berry, J.P., Escaig, F., Lange, F. and Galle, P. (1986) Lab Invest 55, 109-19.
[118] Fragu, P. and Kahn, E. (1997) Microsc Res Tech 36, 296-300.
[119] Clerc, J., Fourre, C. and Fragu, P. (1997) Cell Biol Int 21, 619-33.
[120] Guerquin-Kern, J.L., Coppey, M., Carrez, D., Brunet, A.C., Nguyen, C.H., Rivalle, C., Slodzian, G. and Croisy, A. (1997) Microsc Res Tech 36, 287-95.
[121] McMahon JM, S.R., McCandlish CA, Brenna JT and Todd PJ (1996) RApid Commun Mass Spectrometry 10, 335-340.
[122] U Seedorf, M.F., R Voss, K Meyer, F Kannenberg, D Meschede, K Ullrich, J Horst, A Benninghoven and G Assmann (1995) Clinical Chemistry 41, 548-552.
[123] McQuaw, C.M., Sostarecz, A.G., Zheng, L., Ewing, A.G. and Winograd, N. (2006) Appl Surf Sci 252, 6716-6718.
[124] McQuaw, C.M., Sostarecz, A.G., Zheng, L., Ewing, A.G. and Winograd, N. (2005) Langmuir 21, 807-13.
[125] Sjovall, P., Lausmaa, J., Nygren, H., Carlsson, L. and Malmberg, P. (2003) Anal Chem 75, 3429-34.
[126] Pacholski, M.L., Cannon, D.M., Jr., Ewing, A.G. and Winograd, N. (1998) Rapid Commun Mass Spectrom 12, 1232-5.
[127] Nygren, H., Borner, K., Hagenhoff, B., Malmberg, P. and Mansson, J.E. (2005) Biochim Biophys Acta 1737, 102-10.
[128] W.Schueler, B. (2001) in: TOF-SIMS:Surface Analysis by Maa Spectrometry, pp. 75-94 (Briggs, J.C.V.D., Ed.).
[129] Urbassek, H.M. (2001) in: ToF-SIMS: Surface Analysis by Mass Spectrometry, pp. 139-159, Kaiserslautern.
[130] Benninghoven A, H., and Niehuis E (1993) Analytical Chemistry 65, 630-639.
[131] Vickerman, B.D.a.N.R. (1989).
[132] Schueler, B.W. (2001) in: TOF-SIMS:Surface Analysis by Mass Spectrometry, pp. 75-94 (Briggs, J.C.V.a.D., Ed.).
[133] Chandra, S., Morrison, G.H. and Beyenbach, K.W. (1997) Am J Physiol 273, F939-48.
[134] Gilmore (2001) in: TOF-SIMS:Surface Analysis by Mass Spectrometry, pp. 261-283.
[135] Roddy, T.P., Cannon, D.M., Jr., Ostrowski, S.G., Winograd, N. and Ewing, A.G. (2002) Anal Chem 74, 4020-6.
[136] Chehade, F. et al. (2005) J Nucl Med 46, 1701-6.

[137] Kollmer, F. (2004) Applied Surface Science 231-232, 153-158.
[138] Benguerba, A.B., S. Della-Negra, J. Depauw, H. Joret, Y. Le Beyec, M.G. Blain, E.A. Schweikert, G. Ben Assayag and P. Sudraud (1991) Nucl. Instrum. Methods Phys. Res.
[139] Van Hama Rita, V.V.L., Adamsa Freddy and Adriaens Annemie (2005) J. Anal. At. Spectrom 20, 1088-1094.
[140] Touboul, D., Halgand, F., Brunelle, A., Kersting, R., Tallarek, E., Hagenhoff, B. and Laprevote, O. (2004) Anal Chem 76, 1550-9.
[141] Touboul, D., Brunelle, A., Halgand, F., De La Porte, S. and Laprevote, O. (2005) J Lipid Res 46, 1388-95.
[142] Weibel, D., Wong, S., Lockyer, N., Blenkinsopp, P., Hill, R. and Vickerman, J.C. (2003) Anal Chem 75, 1754-64.
[143] Fletcher, J.S., Lockyer, N.P., Vaidyanathan, S. and Vickerman, J.C. (2007) Anal Chem 79, 2199-206.
[144] Delcorte (2001) in: TOF-SIMS: Surface Analysis by Mass Spectrometry, pp. 161-194.
[145] Gusev, C.a.H. (1998) JOURNAL OF MASS SPECTROMETRY 33, 480-485.
[146] Nygren, H. and Malmberg, P. (2004) J Microsc 215, 156-61.
[147] Morrison, D.P.L.G.H. (1980) 52, 277-280.
[148] Morrison, P.K.C.G.H. (1982) 54, 2111.
[149] Harris, W.C., Jr., Chandra, S. and Morrison, G.H. (1983) Anal Chem 55, 1959-63.
[150] Muddiman, D.C., Gusev, A.I., Proctor, A., Hercules, D.M., Venkataramanan, R. and Diven, W. (1994) Anal Chem 66, 2362-8.
[151] Muddiman David C, G.I., Martin Lee B, Hercules David M. (1996) Fresenius' Journal of Analytical Chemistry 354.
[152] Clark, M.B., Jr. and Gardella, J.A., Jr. (1990) Anal Chem 62, 870-5.
[153] Ostrowski, S.G., Van Bell, C.T., Winograd, N. and Ewing, A.G. (2004) Science 305, 71-3.
[154] Ostrowski, S.G., Kurczy, M.E., Roddy, T.P., Winograd, N. and Ewing, A.G. (2007) Anal Chem 79, 3554-60.
[155] Jeusset, J., Stelly, N., Briancon, C., Halpern, S., Roshani, M. and Fragu, P. (1995) J Microsc 179, 314-20.
[156] Hindie, E., Coulomb, B. and Galle, P. (1992) Biol Cell 74, 89-92.
[157] Grignon, N. (1997) J Microsc 186, 51-66.
[158] Studer, D., Hennecke, H., Müller, M (1992) Planta 188, 155–163.
[159] Somlyo, A.P., Bond, M. and Somlyo, A.V. (1985) Nature 314, 622-5.
[160] Studer, D., Graber, W., Al-Amoudi, A. and Eggli, P. (2001) J Microsc 203, 285-94.
[161] Xia, N. and Castner, D.G. (2003) J Biomed Mater Res A 67, 179-90.
[162] Wold, E.a.G. (1987) Chemometrics and Intellegent Laboratory Sysmtems 2, 37-52.
[163] Bernard W. Agranoff, J.A.B., and Amiya K. Hajra (1999) in: Basic Neurochemistry Molecular, Cellular and Medical Aspects Sixth Edition (Uhler, G.J.S.B.W.A.S.K.F.R.W.A.M.D., Ed.).
[164] X. Vanden Eynde *, P.B. (1998) Surface and Interface Analysis 25, 878 - 888.
[165] Tyler, B.J., Rayal, G. and Castner, D.G. (2007) Biomaterials 28, 2412-23.
[166] Lodisch, B., Zipursky, Matsudaira, Baltimore, Darnell (1999) in: MOLECULAR CELL BIOLOGY.
[167] McDonnell, L.A., Piersma, S.R., MaartenAltelaar, A.F., Mize, T.H., Luxembourg, S.L., Verhaert, P.D., van Minnen, J. and Heeren, R.M. (2005) J Mass Spectrom 40, 160-8.
[168] Rost D., S.T., Wies C., and Jessberger E. K (1999) Meteorit. Planet. Sci. 34, 637–646.
[169] Warley, A. and Skepper, J.N. (2000) J Microsc 198, 116-23.

[170] Chandra, S. and Morrison, G.H. (1992) Biol Cell 74, 31-42.
[171] Arner, P. (2002) Diabetes Metab Res Rev 18 Suppl 2, S5-9.
[172] Scow, R.O., Stricker, F.A., Pick, T.Y. and Clary, T.R. (1965) Ann N Y Acad Sci 131, 288-301.
[173] Edens, N.K., Leibel, R.L. and Hirsch, J. (1990) J Lipid Res 31, 1351-9.
[174] Aas, V., Rokling-Andersen, M., Wensaas, A.J., Thoresen, G.H., Kase, E.T. and Rustan, A.C. (2005) Acta Physiol Scand 183, 31-41.
[175] Forouhi, N.G., Jenkinson, G., Thomas, E.L., Mullick, S., Mierisova, S., Bhonsle, U., McKeigue, P.M. and Bell, J.D. (1999) Diabetologia 42, 932-5.
[176] Connellan, J.M. and Masters, C.J. (1965) Biochem J 94, 81-4.
[177] Clarke, M.S., Vanderburg, C.R., Bamman, M.M., Caldwell, R.W. and Feeback, D.L. (2000) J Appl Physiol 89, 731-41.
[178] Fiehn, W., Peter, J.B., Mead, J.F. and Gan-Elepano, M. (1971) J Biol Chem 246, 5617-20.
[179] Masoro, E.J., Rowell, L.B., McDonald, R.M. and Steiert, B. (1966) J Biol Chem 241, 2626-34.
[180] El Hafidi, M., Valdez, R. and Banos, G. (2000) Clin Exp Hypertens 22, 99-108.
[181] Bulfield, G. (1972) Genet Res 20, 51-64.
[182] Winand, J., Furnelle, J. and Christophe, J. (1968) Biochim Biophys Acta 152, 280-92.
[183] Haessler, H.A. and Crawford, J.D. (1965) Ann N Y Acad Sci 131, 476-84.
[184] Enser, M. (1975) Biochem J 148, 551-5.
[185] Storlien, L.H., Baur, L.A., Kriketos, A.D., Pan, D.A., Cooney, G.J., Jenkins, A.B., Calvert, G.D. and Campbell, L.V. (1996) Diabetologia 39, 621-31.
[186] Storlien, L.H., Pan, D.A., Kriketos, A.D., O'Connor, J., Caterson, I.D., Cooney, G.J., Jenkins, A.B. and Baur, L.A. (1996) Lipids 31 Suppl, S261-5.
[187] Dobrzyn, A. and Ntambi, J.M. (2004) Trends Cardiovasc Med 14, 77-81.
[188] Phinney, S.D., Davis, P.G., Johnson, S.B. and Holman, R.T. (1991) Am J Clin Nutr 53, 831-8.
[189] Bessesen, D.H., Vensor, S.H. and Jackman, M.R. (2000) Am J Physiol Endocrinol Metab 278, E1124-32.
[190] Roddy, T.P., Cannon, D.M., Jr., Ostrowski, S.G., Ewing, A.G. and Winograd, N. (2003) Anal Chem 75, 4087-94.
[191] Milillo Tammy M, G.J.A.
[192] David C Muddiman, A.I.G., Andrew Proctor, and David M Hercules (1994) Anal Chem 66, 2366-2368.
[193] Hansong Cheng, P.A.C.C., and Scott D. Hanton (2000) J. Phys. Chem. A, 18195-1501.
[194] Parks, E.J., Krauss, R.M., Christiansen, M.P., Neese, R.A. and Hellerstein, M.K. (1999) J Clin Invest 104, 1087-96.
[195] Rhoads, G.G., Gulbrandsen, C.L. and Kagan, A. (1976) N Engl J Med 294, 293-8.
[196] Barter, P. (2005) European heart journal Supplements 7, F4-F8.
[197] Willett, W.C. (2000) Proc Soc Exp Biol Med 225, 187-90.
[198] Nasledova, I.D., Fashchevskaia, I.A., Khmel'nitskaia, T.O. and Shaposhnikova, E.S. (1976) Biull Eksp Biol Med 82, 1297-8.
[199] Turner, J., McLennan, P.L., Abeywardena, M.Y. and Charnock, J.S. (1990) Atherosclerosis 82, 105-12.
[200] Zilversmit, D.B. and Shea, T.M. (1989) J Lipid Res 30, 1639-46.
[201] Zilversmit, D.B. (1995) Clin Chem 41, 153-8.
[202] Tall, A.R. (2008) J Intern Med 263, 256-73.
[203] Baird, J.P., Grill, H.J. and Kaplan, J.M. (1997) Am J Physiol 272, R1454-60.

[204] Skilton, M.R., Gosby, A.K., Wu, B.J., Ho, L.M., Stocker, R., Caterson, I.D. and Celermajer, D.S. (2006) Clin Sci (Lond) 111, 281-7.
[205] Malmberg, P., Borner, K., Chen, Y., Friberg, P., Hagenhoff, B., Mansson, J.E. and Nygren, H. (2007) Biochim Biophys Acta 1771, 185-95.
[206] Modrak, J.B. and Langner, R.O. (1980) Atherosclerosis 37, 211-8.
[207] Tufa, K. (2005).
[208] Byfield, F.J., Aranda-Espinoza, H., Romanenko, V.G., Rothblat, G.H. and Levitan, I. (2004) Biophys J 87, 3336-43.